Modeling Convective Drying of Food Products:The Case Study of Yacon (Smallanthus sonchifolius)

Bianca C. Marques
Universidade de São Paulo
Denis Flick
University of Paris-Saclay
Carmen C. Tadini
Universidade de São Paulo
Artemio Plana-Fattori (artemio.planafattori@agroparistech.fr)
University of Paris-Saclay

Research Article

Keywords: convective drying, shrinkage, water diffusion, yac´on

Posted Date: March 26th, 2023

DOI: https://doi.org/10.21203/rs.3.rs-2720541/v1

Additional Declarations: No competing interests reported.

Modeling Convective Drying of Food Products: The Case Study of Yacón (*Smallanthus sonchifolius*)

Bianca C. Marques[1,2], Denis Flick[3], Carmen C. Tadini[1,2] and Artemio Plana-Fattori[3*]

[1]Universidade de São Paulo, Escola Politécnica, Chemical Engineering Department, Main Campus, Butantã, 05508-010 São Paulo, SP, Brazil.

[2]Universidade de São Paulo, FoRC/NAPAN Food Research Center, 05508-010 São Paulo, SP, Brazil.

[3*]Université Paris-Saclay, INRAE, AgroParisTech, UMR SayFood, 91123 Palaiseau, France.

*Corresponding author(s). E-mail(s): artemio.planafattori@agroparistech.fr; Contributing authors: biancacm1@usp.br; denis.flick@agroparistech.fr; catadini@usp.br;

Abstract

The convective drying of a food product whose dehydration occurs under large deformation is studied. A numerical model is proposed for solving the heat and water mass transfer phenomena while accounting for shrinkage. The finite volume method is applied; mesh boundaries move with the dry matter. Shrinkage is predicted from geometrical considerations only, hence no information about the product's mechanical properties is required. Water diffusivity in the product is assumed to depend on both temperature and water content. The approach is illustrated for cylindrical samples of yacón, associated with high water content in *natura* and significant volume reduction after drying. This study considers previous experimental work with a convective drying pilot unit under controlled air temperature and relative humidity conditions. Numerical results reveal, firstly, that the significant evolutions of sample volume (to about 10 % of initial value) and of total water content (to less than 5 % of initial value) are quite well represented. Secondly, despite the relative homogeneity of temperature field, the water content exhibits differences between the sample surface and its core even after six hours of drying. Sensitivity tests put in evidence the major role played by the convective heat and mass transfer coefficients. The physical model and the numerical approach can be adapted in order to predict the evolution of materials with high water content *in natura*, which experience large deformation during the convective drying process.

Keywords: convective drying, shrinkage, water diffusion, yacón

1 Introduction

Drying commonly describes the process of thermally removing volatile substances to yield a solid product. The first objective of dehydration of food materials is to reduce the potential for growth and metabolic activity of microorganisms, as a way to increase the accessibility of food products beyond harvesting conditions. Other objectives are to enhance its quality; to ease its handling; and to allow further processing (Sokhansanj & Jayas, 2006).

When a wet solid is subjected to thermal drying, two processes occur simultaneously: 1) transfer of energy (heat) from the surrounding environment to evaporate the surface moisture, and 2) transfer of internal moisture to the surface of the solid and its subsequent evaporation due to process 1. The rate at which drying is accomplished is governed by the rate at which the two processes proceed. Heat transfer from the surrounding environment to the wet solid can occur as a result of convection, conduction, or radiation and in some cases as a result of a combination of these effects. For convective hot air drying, the removal of water as vapor from the material surface depends on the external conditions (temperature, humidity and flow of drying air), and on the area of exposed surface. The mobility of moisture within the product is a function of its temperature and water content. In a drying operation, heat or mass transfers may be the limiting factor governing the rate of drying, although they both proceed simultaneously throughout the drying cycle. Following these coupled transfers, spatial fields of water content and temperature develop inside the product. Understanding these transfer aspects is the primary objective of most works published in the field of drying because they enable useful indicators of the drying process to be addressed, such as the drying time, the effect of product size, and the energy consumption. The drying could be partly addressed as well, for example the chemical degradation due to the coupled effect of hydric and thermal activation over time. Due to the strong coupling and the non-linear behavior, analytic solutions are available only under strong and somehow unrealistic assumptions: computational simulation is therefore mandatory (Perré *et al.*, 2023).

In the particular case of convective drying, relatively warm dry air flows around cold moist food samples. A simultaneous transfer of both heat and water takes place so that heat is transported from the air to the material, whereas water is transported from the food core, then to its surface, and, eventually, to the air. Theoretical models have been designed for studying the whole ensemble of phenomena; they involve coupled nonlinear partial differential equations that can be solved by cumbersome numerical methods, which are time-consuming and difficult to incorporate in on-line control devices (Ramachandran *et al.*, 2018).

One of the most important physical changes that food materials suffer during drying is the reduction of its volume. Loss of water and heating cause stresses in the cellular structure of the food matrix leading to change in shape and decrease in dimension. Deformation, internal stress, product failure and poor re-hydration are among the major challenges encountered in the drying process. Shrinkage of food materials can be seen as a negative consequence on the quality of the dehydrated product: changes in shape, loss of volume and increased hardness cause in most cases a negative impression on the consumer. There are, on the other hand, some dried products that have had traditionally a shrunken aspect, a requirement for the consumer of raisins, dried plums, peaches or dates (Mayor & Sereno, 2004). Decades of experimental work reveal that shrinkage of food materials under drying is influenced by the product biophysical properties, by the sample size and geometry, by the exposure of the sample to transfer mechanisms, and by the processing approach and its operating conditions (e.g. Mahiuddin *et al.*, 2018).

Fruits and vegetables have a heterogeneous micro-structure which dynamically changes during drying. Currently, food drying models approximate the material's structure through a representative elementary volume which adopts a larger scale of description and considers the fluid phases as fictitious continuum. This assumption limits the ability of the models to capture the heterogeneity of food material. The multi-scale modeling is considered to have the ability to overcome this limitation and advance the understanding of the micro level transport processes; it constitutes an alternative approach to calculate the water diffusivity by explicitly considering the material's heterogeneity rather than the use of a simple empirical relationships. However, multi-scale modeling become very computationally demanding in the case of large deformation, and solution techniques for such a challenging problem remain a subject of investigation (Welsh *et al.*, 2018, 2021). Macro-scale modeling (i.e. continuum-based approach for fluid flow, heat and mass transfer) is the most developed in the food applications; furthermore, this approach has the greatest potential to be integrated into the design process (Datta, 2008). Main challenges for the macro-scale modelling of convective drying of fruits and vegetables are a) the dependence of experimentation to generate parameters of the model, b) the difficulty to include the shrinkage, and c) that the results of the model are dependent on the product and the range of conditions under which it is tested (Castro *et al.*, 2018).

Physics-based modeling can provide better insights into the shrinkage that accompanies simultaneous heat and mass transfer during drying (Castro *et al.*, 2018; Mahiuddin *et al.*, 2018; Chandramohan, 2020). Accounting for shrinkage yields drying rates which are more realistic, and higher, than those obtained in neglecting it (Golestani *et al.*, 2013). With shrinkage, the pathway for water to migrate across the matrix to the surface becomes smaller, leading to a faster water removal (Defraeye and Radu, 2018).

Detailed physics-based models can be closer to reality than simpler approaches, but their solutions are more difficult to reach. A complete thermo-hygro- mechanical model requires, in addition to thermal conductivity and water diffusivity, the knowledge of rheological parameters (Young's modulus, Poisson's coefficient, contraction coefficient due to water loss...). Moreover, especially under large deformation, the food material cannot be considered as purely elastic; plastic or visco- elastic behavior, with additional parameters, should be taken into account. All these mechanical parameters depend on temperature and moisture, and are difficult to measure or estimate (e.g., Curcio *et al.*, 2016; Yuan *et al.*, 2019). Modeling these strongly coupled phenomena (water mass and heat transfer, mechanics) provides a comprehensive and in-depth view of the process: time, cost, and economical value. One could dream at an ideal simulation tool that is able to account for all these coupled transport phenomena, allowing the effect of each parameter to be investigated and the whole process to be improved or even optimized as a function of the expectations of the end-users. However, to achieve this ultimate objective is a long and difficult route (Perré *et al.*, 2023).

Most published drying models do not take shrinkage into account or use a numerical artifice called domain adaptation. This approach considers that the domain is fixed at each computation time step (for heat and mass transfer), and is updated continuously according to geometric global rule. For instance, each node is moved homothetically towards the center of the matrix, to reduce the volume without changing the temperature and water content attached to the node. While this methodology presents good results from an engineering point of view, it is questionable whether it is valid in providing information regarding the phenomena occurring during drying, while undoubtedly useful for design, analysis, and optimization of industrial dryers (Katekawa and Silva, 2006). Recent contributions incorporate experimental assessment of shrinkage in studying the evolution of food products, while allowing the identification of parameters describing the influence of temperature on the water diffusivity in the product (e.g. Brasiello *et al.*, 2021).

Here we present an approach for studying the evolution of food products that can experience significant shrinkage under convective drying. The original contribution here proposed lies in experimental-based geometrical considerations for estimating how shrinkage is locally distributed in different directions. The detailed mechanical behavior of the food material is not required. The approach is implemented in a flexible numerical model which includes i) the coupling between heat and water mass transfer, and ii) the variation of water diffusivity in the food matrix with the temperature and the water content itself. The latter issue deserves special attention: parameters describing the influence of temperature and water content on water diffusivity are identified by comparing model predictions (including shrinkage) and observations of water content. The approach is illustrated for cylindrical slices of yacón (*Smallantus sonchifolius*), a plant cultivated originally in the Andean region for its tuberous, mildly sweet roots. The interest in yacón has increased (Caetano *et al.*, 2016): it constitutes a good option for low- carbohydrate diets because of its low amounts of sucrose and glucose, and its high amount of non- digestible carbohydrates. The industrial utilization of yacón is quite broad (Lebeda *et al.*, 2012). More than 70 % of the fresh tuberous root biomass of yacón is composed of water (Lachman *et al.*, 2003). Water activity is high, suggesting a short shelf-life: partial hydrolysis of fructans can start a few days after harvest (Graefe *et al.*, 2004). Drying is a convenient way to prepare yacón for storage, and the influence of drying conditions on its composition has been investigated (Scher *et al.*, 2009; Campos *et al.*, 2016; Khajehei *et al.*, 2018; Salinas *et al.*, 2018). In the particular case of convective drying, the final color parameters of the dehydrated product (and hence the consumer's perception) can effectively depend on the pre-treatment applied to raw yacón samples (Martins *et al.*, 2022).

Shrinkage cannot be neglected in studying the evolution of yacón submitted to convective drying: the sample shape can be completely modified and the final volume can reach 10 % of initial value (Bernstein & Norena, 2014). Such a finding has not forbidden the assumption of negligible shrinkage of yacón samples in preliminary studies devoted to the physics-based modeling of coupled heat and mass transfer (Perussello *et al.*, 2013, 2014), as well as to the assessment of constant water diffusivity in the product (Shi *et al.*, 2013; Lisboa *et al.*, 2018).

The evolution of yacón samples under convective drying is hereafter studied while coupling heat and mass transfer phenomena, allowing the influence of both temperature and water content on the equivalent water diffusivity in the product; in addition, the sample shrinkage is estimated from geometrical considerations based on previous experimental work (Marques *et al.*, 2022) conducted with a convective drying pilot unit, under controlled air temperature and relative humidity conditions. The present study has as main objective to predict the evolution of temperature and water content depending on the position in yacón samples exposed to convective drying while accounting for their shrinkage. This will allow to investigate not only the effect of various drying conditions (air flow, temperature, humidity) on the drying time (i.e. the productivity of drying equipment) and on the final shape of the sample (say, acceptability by consumer) but also on the local transformation of product (e.g. vitamin degradation, positive/negative neo-formed compounds) which could be assessed by thermo-hygro dependent reactional models. This could help to optimize drying conditions.

2 Heat and Mass Transfer Modeling

The convective drying of a slice of food matrix is hereafter studied by taking into account the following assumptions:

• evaporation occurs at the surface only;
• energy transfer occurs due to heat conduction inside the food matrix and convection at its surface;
• liquid water migrates inside the matrix relatively to dry matter following moisture gradient; and
• no porosity appears during drying.

The last assumption means that, locally, the total volume occupied by the food matrix containing 1 kg of dry matter can be expressed as the sum of volumes that are occupied by dry matter and water:

$$\frac{1}{\rho_{dm}} = \frac{1}{\rho_{dm}^{\#}} + \frac{X_w}{\rho_w^{\#}} \tag{1}$$

wherein ρ_{dm} is expressed in kg of dry matter [kg-dm] by cubic meter of food product; X_w is the water content in the food product, dry basis [kg-w/kg-dm]; and $\rho_{dm}^{\#}$ and $\rho_w^{\#}$ are the intrinsic dry matter and water mass densities.

The conservation equation for the water content can be expressed, in its convective form, as:

$$\frac{\partial X_w}{\partial t} + \vec{v}_{dm} \cdot \vec{\nabla} X_w = \frac{1}{\rho_{dm}} \vec{\nabla} \cdot \vec{j}_{w/dm} \tag{2}$$

wherein $\vec{v}_{dm}$ is the dry matter velocity in the food product. The water flux relative to the dry matter is given by:

$$\vec{j}_{w/dm} = -D_w \vec{\nabla} (\rho_{dm} X_w) \tag{3}$$

wherein D_w is the water diffusivity [m^2/s] in the food product. Equation 2 is solved by taking into account the following boundary condition at the food matrix surfaces:

$$\vec{j}_{w/dm} \cdot \vec{n} = k \left(a_w\{X_w\}\, C_{sat}\{T\} - RH_{air}\, C_{sat}\{T_{air}\} \right) \tag{4}$$

wherein k is the mass transfer coefficient [m/s], $a_w\{X_w\}$ is the water activity in the product at the water content X_w, and $C_{sat}\{T\}$ is the saturated water vapor concentration [kg-w/m^3] at the temperature T.

The internal energy of the food product (by kg of dry matter) is the sum of the internal energies of dry matter and water:

$$u = u_{dm} + X_w u_w = \left(C_{dm}^{\#} + X_w C_w^{\#} \right) T \tag{5}$$

wherein $C_{dm}^{\#}$ and $C_{w}^{\#}$ are the dry matter and water heat capacities. The conservation equation for the internal energy can be expressed as:

$$\frac{\partial u}{\partial t} + \vec{v}_{dm} \cdot \vec{\nabla} u = \frac{1}{\rho_{dm}} \left(\vec{\nabla} \cdot \vec{j}_{w/dm} \, u_w + \vec{\nabla} \cdot \vec{j}_q \right) \tag{6}$$

wherein the energy flux is given by:

$$\vec{j}_q = -\lambda \vec{\nabla} T \tag{7}$$

wherein λ is the bulk thermal conductivity, obtained as $\lambda = (\lambda_{dm}^{\#})^{\alpha} (\lambda_{w}^{\#})^{(1-\alpha)}$; $\lambda_{dm}^{\#}$ and $\lambda_{w}^{\#}$ are the intrinsic dry matter and water thermal conductivity values, and α is the volume fraction occupied by dry matter in the food matrix, given by $1/(1 + \rho_{dm}^{\#} X_w / \rho_{w}^{\#})$.

Equation 6 is solved by taking into account the following boundary condition at the food matrix surfaces:

$$\vec{j}_q \cdot \vec{n} = h \, (T - T_{air}) + L_v \, \vec{j}_{w/dm} \cdot \vec{n} \tag{8}$$

wherein h is the heat transfer coefficient [W/m^2/K] and L_v is the latent heat of water vaporization [J/kg].

Water diffusivity D_w in the product is required for evaluating water migration inside the food matrix (equation 3). The two-phase model proposed by Maroulis *et al.* (2001) is used:

$$D_w\{X_w, T\} = \frac{1}{1 + X_w} D_{w,dry}\{T\} + \frac{X_w}{1 + X_w} D_{w,wet}\{T\} \tag{9}$$

$$D_{w,dry}\{T\} = D_{w,dry,ref} \exp\left(- \frac{E_{dry}}{R} \left(\frac{1}{T} - \frac{1}{T_{ref}} \right) \right) \tag{10}$$

$$D_{w,wet}\{T\} = D_{w,wet,ref} \exp\left(- \frac{E_{wet}}{R} \left(\frac{1}{T} - \frac{1}{T_{ref}} \right) \right) \quad . \tag{11}$$

Activation energy values E_{dry} and E_{wet} for diffusion in very dry ($X_w << 1$) and very wet material ($X_w >> 1$) were both assumed to be 30 kJ/mol, from experimental convective drying of yacón (Shi *et al.*, 2013). Reference temperature T_{ref} was chosen equal to 333.15 K (60 °C). Diffusivity values in very dry ($D_{w,dry,ref}$) and in very wet material ($D_{w,wet,ref}$) at the reference temperature were identified by comparing observations and model predictions of dimensionless water content in the whole food matrix ($\overline{X}_w^{\star} = \overline{X}_w / X_{w,0}$).

Water activity a_w in the product is required for evaluating surface evaporation (equation 4). Experimental work has provided measurements of water content as a function of the water activity in slices of yacon (Figure 2 of Marques *et al.*, 2022); those measurements were approximated by the

Guggenheim-Anderson-deBoer (GAB) model:

$$X_w = \frac{C\, K\, X_{w,mono}\, a_w}{(1 - K\, a_w)\,(1 - K\, a_w + C\, K\, a_w)} \tag{12}$$

Parameters were identified from desorption measurements of yacón samples (see Table 3 of Marques *et al.*, 2022).

Mass k and heat h transfer coefficients are required for evaluating water mass and energy fluxes at the surface (equations 4 and 8). On one hand, the ratio h/k was estimated after invoking the heat and mass transfer analogy, through the expression $\rho_{air}\, C_{P,\,air}\, Le^{2/3}$ (Incropera *et al.*, 2003, pp.410-411). Lewis number was computed as the ratio of the thermal diffusivity of air to the mass diffusivity of water vapor in the air. On the other hand, the heat transfer coefficient was estimated after assuming that all the incoming heat is translated into evaporation at the wet-bulb temperature at the beginning of drying when the surface is wet ($a_w \simeq 1$) (McCabe *et al.*, 2014, p.807). Such an assumption allowed the following expression:

$$h = \frac{m_{dm}\, L_v}{S_0\, (T_{air} - T_{wb})} \left(\frac{d\overline{X}_w}{dt}\right)_{t=0} . \tag{13}$$

This equation involves the initial values of the whole surface S_0 of the product slice and of the time derivative of water content $(d\overline{X}_w/dt)|_{t=0}$. The latter was identified from analysis of observations of water content during drying experiments, for each of operating conditions here considered (see equation 13 and Table 4 of Marques *et al.*, 2022).

Tables 1 and 2 summarize the drying operating conditions taken into account as well as the product and water thermo-physical properties considered, among other key parameters required by the numerical model.

3 Shrinkage Modeling

The crux of our approach is the representation of shrinkage, as a consequence of evaporation at the surface and water migration within the food matrix. Insight about the shrinkage of yacón comes from a companion study (Marques *et al.*, 2023). The drying behavior of yacón samples at cellular level was observed in Environmental Scanning Electron Microscope images; the most striking result is the collapse of elliptical-shaped cells during drying. The similarity between volumetric water loss and total volume loss suggests that the porosity of yacón is likely to be negligible. In other words, the total volume reduction equals the volume of removed water. These findings justify equation 1. Such an assumption has been considered in previous studies devoted to drying of selected fruits and vegetables (Raghavan *et al.*, 1995; Sabarez, 2012).

The macroscopic perspective of the problem is featured in Figure 4 of Marques *et al.* (2022), which displays experimental values of the dimensionless diameter $D^\star = D/D_0$ of yacón slices under selected drying conditions.

The possible influence of drying conditions seemed shadowed by experimental uncertainties. That Figure compared observations with hypothetical shrinkage behavior of the form

$$D^\star = (V^\star)^\beta \iff S^\star = (V^\star)^{2\beta} \; ; \; S = \pi \, D^2 / 4 \tag{14}$$

where $V^\star = V/V_0$ is the dimensionless volume and $S^\star = S/S_0$ is the dimensionless horizontal surface. Isotropic shrinkage ($\beta = 1/3$) could be excluded. A more realistic representation for the shrinkage behavior can be reached in focusing the attention on the values of slice diameter and volume under vanishing water content. On one hand, for the fully dried matrix ($X_w \to 0$), observations suggest that $D^\star \sim 0.6$. On the other hand, the application of equation 1 to the condition $X_w \to 0$ and later to $X_w = X_{w,0}$ provides $V^\star \sim 0.05$. Combining these results in equation 14, we reach a value close to $\beta = 1/6$, which is considered in the calculation of diameter reduction in the numerical model. This means that the diameter reduces much less than the height during shrinkage.

The microscopic perspective of the problem is featured in Figure 1. In the beginning (left-hand displays), the food matrix is assumed to have a cylindrical shape with total radius R_0 and total height H_0. The matrix is assumed to be steadily exposed to a uniform transfer of heat and mass across all its surfaces, suggesting the adoption of the same value for the heat transfer coefficients at the upper, lower and lateral surfaces. The lower boundary of the domain corresponds to the plane of symmetry which divides the matrix into two identical halves. The domain is subdivided into a number of control volumes: they constitute rectangular rings, characterized by their initial radius r_0 and by their elementary values of width δr_0, height δz_0, horizontal surface δS_0, and volume δV_0.

With the occurrence of drying (right-hand displays in Figure 1), liquid water is assumed to migrate inside the matrix relatively to the dry matter, while appearance of porosity is neglected. Control volumes deform following the dry matter (the mass of dry matter remains constant in each control volume along drying); their volume decreases and their shape can be distorted. Shrinkage of the product matrix, as assessed by changes in geometric characteristics r, δr, δz, δS and δV, can be different depending on the position of the control volume under consideration.

The vicinity of the plane of symmetry ($z \sim 0$) corresponds to the highest water content values in the matrix; these positions are the last to be dried and hereafter they can be assumed to constitute the "backbone" of the slice. Near to the symmetry plane shrinkage along the radial direction is characterized by the decrease in elementary horizontal surfaces ($\delta S/\delta S_0 < 1$) and radii ($\delta r/\delta r_0 < 1$), and both depend on the decrease of elementary volumes:

$$\frac{\delta S}{\delta S_0} = \frac{2 \, \pi \, r \, \delta r}{2 \, \pi \, r_0 \, \delta r_0} = \left(\frac{\delta V}{\delta V_0} \right)^{2\beta}_{z=0} . \tag{15}$$

This equation, considered in the vicinity of the plane of symmetry ($z \sim 0$), constitutes a local translation of the empirical relationship (14).

It is assumed that the same radial evolution applies whatever the z position. Figure 1 put in evidence that elementary volumes can become trapezoidal rings along the drying period. Shrinkage along the axial (vertical) direction is characterized by the decrease in elementary heights ($\delta z/\delta z_0 < 1$), which depends on the decrease in elementary volumes and horizontal surfaces:

$$\frac{\delta z}{\delta z_0} = \left(\frac{\delta V}{\delta V_0}\right) / \left(\frac{\delta S}{\delta S_0}\right) . \tag{16}$$

Finally, elementary volumes before drying (δV_0) and later on (δV) can be related via the corresponding values of the mass density of the dry matter:

$$\frac{\delta V}{\delta V_0} = \frac{1/\rho_{dm}}{1/\rho_{dm,0}} , \tag{17}$$

wherein mass densities of dry matter are related through equation 1 to the local water content X_w, which constitutes the solution of the conservation equation 2.

The numerical solving of coupled phenomena of heat and water mass transfer while accounting for shrinkage is summarized in the Appendix.

4 Results and Discussion

4.1 Reference Drying Condition: Influence of Key Model Parameters

Looking for the application of the numerical model in the prediction of water content values along the drying period, two key parameters involved in the model of Maroulis *et al.* (2001) remained to be identified (see equations 9 to 11): the water diffusivity values $D_{w,dry,ref}$ in very dry ($X_w << 1$) and $D_{w,wet,ref}$ for very wet material ($X_w >> 1$) at the reference temperature. These parameters were identified by comparing model predictions and observations of water content conducted only under the reference drying condition: air flow 4 m/s, T_{air} = 60 °C, and RH_{air} = 20 % (case A in Table 1) (see Marques *et al.*, 2022).

Figure 2a displays observations of water content conducted under this drying condition. A quite linear decrease of water content with time can be recognized up to about $t_{1/2} \simeq$ 1h15min, when the average water content is half of its initial value ($\overline{X}_w^\star = \overline{X}_w/X_{w,0} = 1/2$). Along this "constant drying rate" period, the product surface remains wet ($a_w \sim 1$), and the drying rate depends on external conditions only. Later on, diffusion from core to surface becomes limiting, whose importance depends on the product structure and characteristics (Mujumdar, 2006). As shown in Figure 2a, the drying time $t_{1/8} \simeq$ 3h10min (when $\overline{X}_w^\star = 1/8$) is clearly out of the constant drying rate period and its value constitutes a complementary information about the drying kinetics. Figure 2a indicates both drying times, according to observations.

The black line in Figure 2a features model predictions reached after assuming, in equations 9 to 11, the values $D_{w,dry,ref} = 10^{-12}$ m^2/s and $D_{w,wet,ref} = 1.6\ 10^{-10}$ m^2/s. These values were identified by minimizing the difference between predicted and observed drying times $t_{1/2}$ and $t_{1/8}$; the application of these values allows differences smaller than 5 min between model predictions and observations. The vanishing value of the water diffusivity in very dry material is consistent with the product structure, nearly crumbly / brittle, after six hours of drying. Water content values as predicted by the numerical model agree fairly well with observations.

The presented model predictions were obtained for a time step of 0.01s and a mesh of 150 elements ($I = 30$, $J = 5$). As shown in Figures 2b and 2c, using different time steps or higher numbers of mesh elements did not change sensibly the results in terms of $t_{1/2}$ and $t_{1/8}$.

Table 3 and Figure 3 summarizes sensitivity tests considering changes on selected physical parameters. Case A represents the model predictions under the reference drying conditions. Cases [A1,... A4] , [A5,... A8] and [A9,... A12] consider variations on parameters $D_{w,dry,ref}$, $D_{w,wet,ref}$, $E_{dry} = E_{wet}$ of the model proposed by Maroulis *et al.* (2001). Values for the water diffusivity in very dry and very wet material correspond to the reference temperature of 60 °C. Cases [A13,... A18] consider variations on the heat transfer coefficient h, which values depend on the drying conditions (see Table 2).

Variations in the range -50 to $+50$ % on the value of water diffusivity in very dry material $D_{w,dry,ref}$ lead to negligible influence on drying times $t_{1/2}$ and $t_{1/8}$. Such a finding can be explained by the huge difference of magnitude (two orders of magnitude) between $D_{w,dry,ref}$ and $D_{w,wet,ref}$, the latter being dominant in equation 9. Variations in the range -50 to $+50$ % on the values assumed for $D_{w,wet,ref}$ or $E_{dry} = E_{wet}$ significantly degrade the reliability of model predictions. It must be noted that these two parameters influence in opposite way the model predictions. On one hand, increasing the water diffusivity in very wet material provides a decreasing tendency for drying times $t_{1/2}$ and $t_{1/8}$ (Figure 3b). Lower (higher) values than the identified value 1.6 10^{-10} m^2/s reduce (increase) water migration relatively to model predictions; this is particularly evident for drying time $t_{1/8}$, which is out of the constant drying rate period. On the other hand, increasing the energy of activation allows a stronger influence of temperature on water diffusion inside the product matrix. Increasing the energy of activation provides an increasing tendency for $t_{1/2}$ and $t_{1/8}$, since the product temperature is always lower than the air temperature (60 °C) which was chosen as the reference one; increasing $E_{dry} = E_{wet}$ thus lowers, in the average, the equivalent water diffusivity in the product. Such a tendency is weaker in the case of $t_{1/2}$, whose values are primarily driven by ambient conditions under which the product is submitted to drying (Figure 3c).

4.2 Reference Drying Condition: Evolution of the Product

Figure 4 displays the temperature, water content, water activity and water diffusivity fields throughout the food slice at selected times. A remarkable result is the thermal homogeneity of the product slice, during the whole drying period. An explanation is provided by the low values of the Biot number $h(H/2)/\lambda$; its decreasing tendency (0.2 down to 0.06) is due to a decrease in height (0.007 down to 0.001 m) which is stronger than in thermal conductivity (0.6 down to 0.3 W/m/K). As expected, evaporation at the surface drives the water migration across the food slice. The lateral surface of the slice experiences faster drying than its upper surface. After six hours under the convective drying conditions here considered, the slice volume decreased to about 7 % of its initial value. Water diffusivity varies with time and space following a complex pattern. At the slice surface, its decreasing tendency is driven by the moisture reduction. The influence of temperature decreases along the drying period, as the slice approaches the ambient temperature 60 °C. Water activity remained high after four hours, over 0.9 throughout large portions of the product slice, suggesting favorable conditions to selected micro-organisms. These results indicate the importance of the latest hours of drying in effectively reducing the water activity at the the slice core. The time and spatial distributions displayed in Figure 4 put in evidence i) the strong coupling between heat and water mass transfer phenomena during the convective drying of a food slice and ii) how the water diffusivity and water activity evolve throughout a food matrix exposed to convective drying under large deformation.

Beyond the two-dimensional fields displayed at selected drying times, the approach allows studying the time evolution at given positions. Figure 5 presents selected properties at two positions along the axis of symmetry of the food slice: at the surface (1) and the core (2). Position 1 moves along with the shrinkage history, being always located at the slice surface; it is exposed to moisture gradients that are stronger than those at position 2. Figure 5a reveals that these positions follow almost the same temperature history; such a finding comes from a combination of the small distance separating these positions and high thermal conductivity in the product. Beginning at $T_0 = 20$ °C, the temperature quickly reaches the wet-bulb temperature (about 34 °C), allowing favorable conditions to evaporation at the surface. Figure 5b presents the water content history at these positions. Convective drying is effective: after 1.5h, there remains about 2.5 % of the initial water content at the surface. At this time, drying really starts at the core, following a slow-fast-slow decreasing tendency. After six hours of drying there remains about 3 % of the initial water content at the core. The evolution of water activity (Figure 5c) is delayed with respect to that of water content. The water activity is not homogeneous throughout the product slice, even after six hours of convective drying. The activity at the surface remains near to 1 (> 0.9) only during a period of about 30min. During this period, the temperature remains near the wet-bulb one (34 °C), and the drying rate is nearly constant. From 30 min to 1h15min, the water activity at surface decrease to 0.7 and the temperature rises to 40 °C. This indicates that diffusion from core to surface is no more sufficient to ensure free water evaporation at surface. However, the temperature difference between the surrounding air and the product surface — which drives the convective heat transfer to the product — decreases only from $T_{air} - T_{wb} = 26$ °C to $T_{air} - 40$ °C $= 20$ °C. This makes that drying rate seems almost constant up to 1h15min, which corresponds very closely to $t_{1/2}$ (when $\overline{X}^{\star}_{w} = 1/2$).

Water diffusivity in the product is assumed to depend on both temperature and moisture, whose relative importance evolves as heating and drying progress with time. Figure 5d shows that, at the surface (position 1), water diffusivity sharply increases when drying starts because temperature increases from $T_0 =$ 20 °C to T_{wb} = 34 °C, and then decreases from 4 10^{-11} to 7 10^{-12} m^2/s because water content decreases from 11 to 0.04 kg-w/kg-dm. At the core (position 2), the water diffusivity follows an increasing tendency until drying significantly occurs therein (after about three hours of drying), corresponding to temperatures about 48 °C; later on, the influence of moisture reduction becomes dominant.

Previous results have discussed the evolution of key variables along the drying time as predicted by the numerical model, either throughout the 2D computational domain (Figure 4) or at selected positions (Figure 5). Additional insight can be attained studying model results as function of the total water content present in the matrix. Figures 6a and 6b compare model predictions with the measurements of dimensions of yacón slices as obtained by Marques *et al.* (2022) under the reference drying conditions [air flow 4 m/s, T_{air} = 60 °C, RH_{air} = 20 %] . The numerical model captures the decreasing tendency of slice diameter, which is very weak during a considerable period (i.e. down to about $\overline{X}^{\star}_{w} \sim 0.3$). The decreasing tendency of slice height is almost linear during such a period. The comparison of model predictions with measurements of slice height is difficult: the initial flat character of the upper and lower surfaces of the samples progressively disappears along the drying (see Figure 1 of Marques *et al.*, 2022), turning somewhat ambiguous the notion of slice height. Figure 6c presents the total surface reduction along the drying. A first decreasing tendency can be recognized from the beginning down to $\overline{X}^{\star}_{w} \sim 0.3$ when the diameter reduction becomes progressively more significant (Figure 6a); towards the end of the drying period, the total surface decreases to about 35 % of its initial value. Figures 6d and 6e show the dimensionless drying kinetics $d\overline{X}^{\star}_{w}/dt$ and $d\overline{X}^{\star}_{w}/dt.S^{\star}$. Both sharply increase when drying starts, while the food product leaves its initial temperature (20 °C) and reaches the wet-bulb temperature (about 34 °C) (Figure 5a). Later on, both drying kinetics decrease. On one hand, the dimensionless evaporative <u>flow</u> $d\overline{X}^{\star}_{w}/dt$ follows a decreasing tendency along drying, following the water activity decrease at the surface (Figure 5c) as well as the total surface decrease (Figure 6c). On the other hand, the dimensionless evaporative <u>flux</u> $d\overline{X}^{\star}_{w}/dt.S^{\star}$ follows a more complex decreasing tendency. Firstly, there is a period ($\overline{X}^{\star}_{w} > 0.7$), along which $d\overline{X}^{\star}_{w}/dt.S^{\star}$ is quite constant: this would be the constant drying rate period according to model predictions, roughly the first hour of drying (Figure 6a). In a second period ($0.7 > \overline{X}^{\star}_{w} > 0.2$), $d\overline{X}^{\star}_{w}/dt.S^{\star}$ decreases quite uniformly, while the water content remains high at the matrix core (Figure 5b). A final period starts when water content at core decreases significantly, at about three hours of drying (i.e. at about $t_{1/8}$).

4.3 Influence of Drying Conditions

Cases [B, C, D] of Tables 1, 2 and 3 correspond to the three other drying conditions considered by Marques *et al.* (2022) in studying the evolution of yacón samples with a convective drying pilot unit. The heat transfer coefficient value was in each case adapted to the ambient conditions but the other parameters (including the water diffusivity in very dry and in very wet material) remain unchanged.

The reliability of model predictions for these three cases is smaller than in case A but remains still acceptable, as put in evidence by the departures $\Delta t_{1/2}$ and $\Delta t_{1/8}$ between model predictions and observations under same drying conditions (see Table 3). The numerical model captures the influence of ambient conditions on the drying times $t_{1/2}$ and $t_{1/8}$: for a given air temperature, they are slightly shorter under $RH_{air} = 20$ % than under $RH_{air} = 30$ % as a consequence of more favorable conditions to evaporation at the food matrix surface at lower air relative humidity (see Table 1).

Figure 7 compares observations and model predictions of water content under the four drying conditions. The difficulty of such comparison is evident under the drying conditions [air flow 4 m/s, $T_{air} = 60$ °C, $RH_{air} = 30$ %] (case B), which were particularly difficult to conduct from the experimental point of view (see Figure 7b). Drying experiments under $T_{air} = 50$ °C were more successfully repeated (Figures 7c and 7d), allowing more robust conditions to assess the reliability of model predictions for cases C and D. In both cases, the numerical model underestimates the drying rate almost systematically, suggesting that additional efforts are welcome e.g. in the identification of the equivalent water diffusivity.

5 Conclusions

Drying phenomena (water migration inside the matrix, evaporation at its boundaries) cannot be dissociated from the geometrical evolution of the food matrix. A simple approach which does not require a complex mechanical model was proposed for shrinkage. The goal was to estimate how the local volume reduction (due to dehydration) is distributed between axial and radial shrinkage. Our approach assumes that the radial reduction is primarily driven by the decreasing water content of the product situated at the core (near the plane of symmetry of the slice volume). The assessment of such a tendency became possible from careful measurements of the slice diameter.

We demonstrated that convective drying of food slices can be studied with a simple model including shrinkage. In its present implementation, the approach was successfully applied for a case where the volume was divided by about 10 during drying. The algorithm can be adapted, for instance, for including simple reaction kinetics, as a way to predict the influence of drying on chemical properties at different positions of the food matrix.

The model proposed by Maroulis *et al.* (2001) was assumed for approximating the water diffusivity in yacón samples as function of temperature and water content. The values $D_{w,dry,ref} = 1.0\ 10^{-12}$ m^2/s and $D_{w,wet,ref} = 1.6\ 10^{-10}$ m^2/s at 60 °C for very dry and very wet material were identified while accounting for sample shrinkage; however they are not directly comparable with most results available in the literature for yacón samples which were identified after neglecting sample shrinkage (e.g. Perussello *et al.*, 2013, 2014; Shi *et al.*, 2013; Mendonça *et al.*, 2017; Lisboa *et al.*, 2018).

In addition to the water diffusivity in yacón samples, the implementation of the numerical model required a number of other parameters, most of them associated with the drying operating conditions, the thermo-physical properties of the product, and the geometry of the food slice. The influence of selected parameters on the model predictions was analyzed. Variations on the heat transfer coefficient and on the water diffusivity in very wet material were the most important, which was somewhat expected because the major role played by these parameters in heat and water mass transfer phenomena.

Future work should assess the reliability of this approach under other convective drying conditions. Testing this approach should consider wider ranges of ambient conditions (air flow, temperature and relative humidity) and other raw food products. Much work remains to be done in order to clarify the relationship between shrinkage and moisture loss.

Acknowledgments. We warmly acknowledge AgroParistech and UMR SayFood for kindly receiving the first named author for a one-year research internship.

Declarations

- Funding
  Authors Bianca Cristine Marques and Carmen Cecilia Tadini received grants from Brazilian agencies: grants 2018 / 21327-1, 2019 / 21832-0, and 2013 / 07914-8 from the São Paulo Research Foundation (FAPESP); finance code 001 from the Coordination for the Improvement of Higher Education Personnel (CAPES); and grant 309548 / 2021 from the National Council for Scientific and Technological Development (CNPq).
- Conflict of interest/Competing interests
  All authors certify that they have no affiliations with or involvement in any organization or entity with any financial interest or non-financial interest in the subject matter or materials discussed in this manuscript.
- Ethics approval
  Not applicable.
- Consent to participate

Not applicable.
- Consent for publication
Not applicable.
- Availability of data and materials
Not applicable.
- Code availability
Not applicable.
- Authors' contributions
B.C. Marques: Methodology, Experimental work, Model improvement, Writing.
D. Flick: Conceptualization, Methodology, Original coding, Manuscript review.
C.C. Tadini: Supervision, Project administration, Funding acquisition, Manuscript review.
A. Plana-Fattori: Methodology, Model improvement, Writing including final review and edition.

References

Bernstein, A., Norena, C. P. Z. (2014). Study of thermodynamic, structural, and quality properties of yacón (*Smallanthus sonchifolius*) during drying. *Food and Bioprocess Technology*, 7, 148-160.
https://doi.org/10.1007/s11947-012-1027-y

Brasiello, A., Venditti, C., Adrover, A. (2021). Non-isothermal moving-boundary model for food drying. *Chemical Engineering Transactions*, 87, 193-198.
https://doi.org/10.3303/CET2187033

Caetano, B. F. R., Moura, N. A., Almeida, A. P. S., Dias, M. C., Sivieri, K., Barbisan, L. F. (2016). Yacón (*Smallanthus sonchifolius*) as a food supplement : Health-promoting benefits of frutooligosaccharides. *Nutrients*, 8, 436.
https://doi.org/10.3390/nu8070436

Campos, D., Aguilar-Galvez, A., Pedreschi, R. (2016). Stability of fructooligosaccharides, sugars and colour of yacón (*Smallanthus sonchifolius*) roots during blanching and drying. *International Journal of Food Science and Technology*, 51, 1177-1185.
https://doi.org/10.1111/ijfs.13074

Castro, A. M., Mayorga, E. Y., Moreno, F. L. (2018). Mathematical modelling of convective drying of fruits: A review. *Journal of Food Engineering*, 223, 152-167.
https://doi.org/10.1016/j.jfoodeng.2017.12.012

Chandramohan, V. P. (2020). Convective drying of food materials: An overview with fundamental aspect, recent developments, and summary. *Heat Transfer*, 49, 1281–1313.
https://doi.org/10.1002/htj.21662

Choi, Y., Okos, M. R. (1986). Effects of temperature and composition on the thermal properties of foods. In M. Le Mageur, P. Jelen (Eds.), *Food Engineering and Process Applications*, pp. 93-101. Elsevier Applied Science.

Curcio, S., Aversa, M., Chakraborty, S., Calabro, V., Iorio, G. (2016). Formulation of a 3D conjugated multiphase transport model to predict drying process behavior of irregular-shaped vegetables. *Journal of Food Engineering*, 176, 36-55.
https://doi.org/10.1016/j.jfoodeng.2015.11.020

Datta, A. K. (2008). Status of physics-based models in the design of food products, processes, and equipment. *Comprehensive Reviews in Food Science and Food Safety*, 7, 121-129.
https://doi.org/10.1111/j.1541-4337.2007.00030.x

Defraeye, T., Radu, A. (2018). Insights in convective drying of fruit by coupled modeling of fruit drying, deformation, quality evolution and convective exchange with air airflow. *Applied Thermal Engineering*, 129, 1026-1038.
https://doi.org/10.1016/j.applthermaleng.2017.10.082

Golestani, R., Raisi, A., Aroujalian, A. (2013). Mathematical modeling on air drying of apples considering shrinkage and variable diffusion coefficient. *Drying Technology*, 31, 40-51.
https://doi.org/10.1080/07373937.2012.714826

Graefe, S., Hermann, M., Manrique, I., Golombek, S., Buerkert, A. (2004). Effects of post-harvest treatments on the carbohydrate composition of yacon roots in the Peruvian Andes. *Field Crops Research*, 86, 157-165.
https://doi.org/10.1016/j.fcr.2003.08.003

Hermann, M., Freire, I., Pazos, C. (1999). Compositional diversity of the yacon storage root. In *Andean Roots and Tuber Crops*, pp.425-432. International Potato Center Program Report 1997-1998, Lima (Peru).

Incropera, F. P., DeWitt, D. P., Bergman, T. L., Lavine, A. S. (2003). *Fundamentals of Heat and Mass Transfer, 7th Edition*. John Wiley & Sons.

Katekawa, M. E., Silva, M. A. (2006). A review of drying models including shrinkage effects. *Drying Technology*, 24, 5-20.
https://doi.org/10.1080/07373930500538519

Khajehei, F., Hartung, J., Graeff-Honninger, S. (2018). Total phenolic content and antioxidant activity of yacón (*Smallanthus sonchifolius*, Poepp. et Endl.) chips : Effect of cultivar, pre-treatment and drying. *Agriculture*, 8, 183. https://doi.org/10.3390/agriculture8120183

Lachman, J., Fernandez, E. C., Orsak, M. (2003). Yacón [*Smallanthus sonchifolius* (Poepp. et Endl.) H. Robinson] chemical composition and use– A review. *Plant Soil and Environment*, 49, 283-290. https://doi.org/10.17221/4126-PSE

Lebeda, A., Dolezalova, I., Fernandez, E., Viehamannova, I. (2012). Yacón (*Asteraceae*; *Smallanthus sonchifolius*). In R. J. Singh (Ed.), *Genetic Resources, Chromosome Engineering, and Crop Improvement, Volume 6 : Medicinal Plants*, pp.641-702. CRC Press.

Lisboa, C. G. C., Gomes, J. P., Figueiredo, R. M. F., Queiroz, A. J. M., Diogenes, A. M. G., Melo, J. C. S. (2018). Effective diffusivity in yacón potato cylinders during drying. *Revista Brasileira de Engenharia Agricola e Ambiental*, 22, 564-569. http://dx.doi.org/10.1590/1807-1929/agriambi.v22n8p564-569.

Mahiuddin, M., Khan, M. I. H., Kumar, C., Rahman, M. M., Karim, M. A. (2018). Shrinkage of food materials during drying: Current status and challenges. *Comprehensive Reviews in Food Science and Food Safety*, 17, 1113-1126. https://doi.org/10.1111/1541-4337.12375

Maroulis, Z. B., Saravacos, G. D., Panagiotou, N. M., Krokida, M. K. (2001). Moisture diffusivity data compilation for foodstuffs: Effect of material moisture content and temperature. *International Journal of Food Properties*, 4, 225-237. https://doi.org/10.1081/JFP-100105189

Marques, B. C., Plana-Fattori, A., Flick, D., Tadini, C. C. (2022). Convective drying of yacón (*Smallanthus sonchifolius*) slices: A simple physical model including shrinkage. *LWT – Food Science and Technology*, 159, 113151. https://doi.org/10.1016/j.lwt.2022.113151

Marques, B. C., Perré, P., Casalinho, J., Tadini, C. C., Plana-Fattori, A., Almeida, G. (2023). Evidence of iso-volume deformation during convective drying of yacón: An extended van Meel model adapted to large volume reduction. *Journal of Food Engineering*, 341, 111311. https://doi.org/10.1016/j.jfoodeng.2022.111311

Martins, A. F. L., Vieira, E. N. R., Leite, B. R. C., Jr., Ramos, A. M. (2022). Use of ultrasound and ethanol to improve the drying of yacón potato (*Smallanthus sonchifolius*) : Effect of chemical and thermal bleaching. *LWT – Food Science and Technology*, 62, 113448.
https://doi.org/10.1016/j.lwt.2022.113448

Mayor, L., Sereno, A. M. (2004). Modelling shrinkage during convective drying of food materials: A review. *Journal of Food Engineering*, 61, 373-386.
https://doi.org/10.1016/S0260-8774(03)00144-4

McCabe, W. L., Smith, J. C., Harriott, P. (2014). *Unit Operations of Chemical Engineering, 7th Edition*. McGraw-Hill.

Mendonça, K., Correa, J., Junqueira, J., Angelis-Pereira, M., Cirillo, M. (2017). Mass transfer kinetics of the osmotic dehydration of yacón slices with polyols. *Journal of Food Processing and Preservation*, 41, e12983.
https://doi.org/10.1111/jfpp.12983.

Mujumbar, A. S. (2006). Principles, classification, and selection of dryers. In A. S. Mujumbar (Es.), *Handbook of Industrial Drying, 3rd Edition*, pp. 4–32. CRC Press.

Perré, P., Rémond, R., Almeida, G., Augusto, P., Turner, I. (2023). State-of-the-art in the mechanistic modeling of the drying of solids: A review of 40 years of progress and perspectives. *Drying Technology*,
doi.org/10.1080/07373937.2022.2159974.

Perussello, C. A., Mariani, V. C., Masson, M. L., Castilhos, F. (2013). Determination of thermophysical properties of yacón (*Smallanthus sonchifolius*) to be used in a finite element simulation. *International Journal of Heat and Mass Transfer*, 67, 1163-1169.
http://dx.doi.org/10.1016/j.ijheatmasstransfer.2013.09.004

Perussello, C. A., Kumar, C., Castilhos, F., Karim, M. A. (2014). Heat and mass transfer modeling of the osmo-convective drying of yacón roots (*Smallanthus sonchifolius*). *Applied Thermal Engineering*, 63, 23-32.
http://dx.doi.org/10.1016/j.applthermaleng.2013.10.020.

Raghavan, G. S. V., Tulasidas, T. N., Sablani, S. S., Ramaswamy, H. S. (1995). A method of determination of concentration dependent effective moisture diffusivity. *Drying Technology*, 13, 1477-1488.
https://doi.org/10.1080/07373939508917034.

Ramachandran, R. P., Akbarzadeh, M., Paliwal, J., Cenkowski, S. (2018). Computational Fluid Dynamics in drying process modelling– A technical

review. *Food and Bioprocess Technology*, 11, 271-292.
https://doi.org/10.1007/s11947-017-2040-y.

Sabarez, H. T. (2012). Computational modelling of the transport phenomena occurring during convective drying of prunes. *Journal of Food Engineering*, 111, 279-288.
https://doi.org/10.1016/j.jfoodeng.2012.02.021.

Salinas, J. G., Alvarado, J. A., Bergenstahl, B., Tornberg, E. (2018). The influence of convection drying on the physicochemical properties of yacón (*Smallanthus sonchifolius*). *Heat and Mass Transfer*, 54, 2951-2961.
https://doi.org/10.1007/s00231-018-2334-2

Scher, C. F., Rios, A. O., Norena, C. P. Z. (2009). Hot air drying of yacón (*Smallanthus sonchifolius*) and its effect on sugar concentrations. *International Journal of Food Science and Technology*, 44, 2169-2175.
https://doi.org/10.1111/j.1365-2621.2009.02056

Sokhansanj, S., Jayas, D. S. (2006). Drying of foodstuffs. In A. S. Mujumbar (Ed.), *Handbook of Industrial Drying, 3rd Edition*, pp. 522–546. CRC Press.

Shi, Q., Zheng, Y., Zhao, Y. (2013). Mathematical modeling on thin-layer heat pump drying of yacón (*Smallanthus sonchifolius*) slices. *Energy Conversion and Management*, 71, 208-216.
https://doi.org/10.1016/j.enconman.2013.03.032

Welsh, Z., Simpson, M. J., Khan, M. I. H., Karim, M. A. (2018). Multiscale modeling for food drying: State of the art. *Comprehensive Reviews in Food Science and Food Safety*, 17, 1293-1308.
https://doi.org/10.1111/1541-4337.12380

Welsh, Z. G., Khan, M. I. H., Karim, M. A. (2021). Multiscale modeling for food drying: A homogenized diffusion approach. *Journal of Food Engineering*, 292, 110252.
https://doi.org/10.1016/j.jfoodeng.2020.110252

Yuan, Y., Tan, L., Xu, Y., Yuan, Y., Dong, J. (2019). Numerical and experimental study on drying shrinkage-deformation of apple slices during process of heat-mass transfer. *International Journal of Thermal Sciences*, 136, 539-548.
https://doi.org/10.1016/j.ijthermalsci.2018.10.042

Appendix: Numerical Solving

The food matrix is represented by a two-dimensional (2D) axis-symmetrical computational domain with total radius R_0 and total height $Z_0 = H_0/2$ before drying starts; H_0 is the (physical) actual height of the food matrix submitted to experimental conditions. The finite volume method is applied, with an explicit scheme, and the domain is subdivided into a number of control volumes (cells). The cells deform following the dry matter: the mass of dry matter remains constant in each cell along drying.

Before drying starts ($t = 0$) all the cells are rectangular. In the present study, the mesh is built considering I and J cells along the radial and the axial directions, respectively; coordinates have the origin at the slice center. The computational domain has an initial aspect ratio $R_0/Z_0 \sim 6$; meshes are chosen in taking $I = 6 \times J$. The (i,j)-th cell is characterized by:

• its initial position $[r_0(i),\, z_0(i,j)]$, required in the evaluation of heat and water mass flows; the position of inner cells is defined as their center, the position of the outer cells is defined at the interface of the domain with surrounding air;
• four vertices, being that $[R_0(i),\ Z_0(i,j)]$ is the position of the left-bottom corner of the (i,j)-th cell; hence $r_0(i) = (R_0(i) + R_0(i+1))/2$ and $z_0(i,j) = (Z_0(i,j) + Z_0(i,j+1))/2$;
• its height $\Delta Z_0(i,j) = Z_0(i,j+1) - Z_0(i,j)$;
• its width $\Delta R_0(i) = R_0(i+1) - R_0(i)$;
• its surface $S_0(i) = \pi\,(R_0(i+1)^2 - R_0(i)^2)$ between two successive radial ordinates; and
• its volume $V_0(i,j)$.

Each cell is associated with a single value for the product temperature and for the water content. In the beginning, initial values T_0 and $X_{w,0}$ are assigned to all the cells. The initial volume $V_0(i,j)$ of each cell is known, hence it is possible to calculate the mass of dry matter $m_{dm}(i,j)$ contained in each cell, which remains constant along drying.

During the drying period ($t > 0$), the food matrix is submitted to convective heating and evaporation at its surface and to heat conduction and water diffusion inside it. Independently on the drying state of the food matrix, all the cells are assumed to be trapezoids, being that their vertical sides are imposed to be parallel to the axis of symmetry; such a condition translates the assumption of a same radial shrinkage to all the cells either near the plane of symmetry or outside it (see Section 3). Figure 8 displays key elements of the 2D axi-symmetric representation of an elementary volume of the food matrix. Temperature and water content values are assumed to be representative of the whole cell, and hence follow indexing of positions $[r(i),\, z(i,j)]$.

After a time step ($\Delta\, t$), the total variation in the water content in the (i,j)-th cell and that in the temperature associated with this cell are calculated as:

$$\begin{aligned}\Delta X_w(i,j) &= (\,(\,(\,\phi_Z(i,j) - \phi_Z(i,j{+}1)\,) \\ &\quad +\,(\,\phi_R(i,j) - \phi_R(i{+}1,j)\,)\,)\,\Delta t\,/\,m_{dm}(i,j) \qquad (18)\\ \Delta T(i,j) &= (\,(\,(\,\Phi_Z(i,j) - \Phi_Z(i,j{+}1)\,) \\ &\quad +\,(\,\Phi_R(i,j) - \Phi_R(i{+}1,j)\,)\,)\,\Delta t\,/\,(\,m_{dm}(i,j)\,C_P(i,j)\,) \qquad (19)\end{aligned}$$

wherein $C_P = C^{\#}_{dm} + X_w C^{\#}_w$. These equations involve water mass and heat flows (ϕ [kg-w/s] and Φ [J/s]) along the axial z- and radial r- directions. In the case of inner cells, the water and energy rates are calculated as:

$$\begin{aligned}\phi_Z(i,j) &= S(i,j)\,D_w(i,j)\,\rho_{dm}(i,j) \\ &\quad \times\,(\,X_w(i,j{-}1) - X_w(i,j)\,)/(\,z(i,j) - z(i,j{-}1)\,) \qquad (20)\\ \phi_R(i) &= 2\,\pi\,\Delta Z(i,j)\,D_w(i,j)\,\rho_{dm}(i,j) \\ &\quad \times\,(\,X_w(i{-}1,j) - X_w(i,j)\,)/(\,\ln(\,r(i)/r(i{-}1)\,)\,) \qquad (21)\\ \Phi_Z(i,j) &= S(i,j)\,\lambda(i,j) \\ &\quad \times\,(\,T(i,j{-}1) - T(i,j)\,)/(\,z(i,j) - z(i,j{-}1)\,) \qquad (22)\\ \Phi_R(i,j) &= 2\,\pi\,\Delta Z(i,j)\,\lambda(i,j) \\ &\quad \times\,(\,T(i{-}1,j) - T(i,j)\,)/(\,\ln(\,r(i)/r(i{-}1)\,)\,)\,. \qquad (23)\end{aligned}$$

Convective drying conditions are assumed to be steady and defined by the air temperature (T_{air}) and relative humidity (RH_{air}). Water and energy rates are calculated at surface cells while respecting the boundary conditions of the problem (equations 4 and 8). For instance, in the case of the lateral surface:

$$\begin{aligned}\phi_R(I{+}1,j) &= k\,\times\,2\,\pi\,r(I,j)\,\Delta Z(I{+}1,j) \\ &\quad \times\,(\,a_w(I,j)\,C_{w,sat}\{T(I,j)\} - RH_{air}\,C_{w,sat}\{T_{air}\}\,) \qquad (24)\\ \Phi_R(I{+}1,j) &= h\,\times\,2\,\pi\,r(I,j)\,\Delta Z(I{+}1,j) \\ &\quad \times\,(\,T(I,j) - T_{air}\,)\,+\,L_v\,\phi_R(I{+}1,j)\,. \qquad (25)\end{aligned}$$

Thus, heat flows Φ at the surface are computed by adding two contributions: the first is proportional to the difference between the temperatures in the product and in the ambient air, the second is proportional to the water mass flow ϕ. This latter requires the water activity, which is estimated at each position of the air-product interface by solving equation 12 while employing the water content available in the previous time step.

The calculation of total variations $\Delta X_w(i,j)$ and $\Delta T(i,j)$ (equations 18 and 19) allows updating the temperature and water content values for each cell. The following sequence of steps allows updating the volume and position of the (i,j)-th cell of the food matrix.

(a) The cell volume comes from equation 1, considering the updated water content value X_w:

$$V(i,j) \;=\; m_{dm}(i,j)\, \left(\frac{1}{\rho^{\#}_{dm}} \;+\; \frac{X_w(i,j)}{\rho^{\#}_{w}} \right) \;,\;\; 1 \leq i \leq I \;,\;\; 1 \leq j \leq J \;. \tag{26}$$

(b) The horizontal surface of all the cells in the plane of symmetry comes from equation 15:

$$\Delta S(i) \;=\; \Delta S_0(i) \left(\frac{V(i,1)}{V_0(i,1)} \right)^{2\beta} \;,\;\; 1 \leq i \leq I \;. \tag{27}$$

(c) The radial ordinate $R(i+1)$ for all the cells situated in a given column (same distance from the axis of symmetry) is obtained as:

$$S(i) \;=\; \pi \; \left(R(i+1)^2 \;-\; R(i)^2 \right) \;,\;\; 1 \leq i \leq I \;, \tag{28}$$

wherein $R(1) = 0$ (axis of symmetry).
(d) The heights at $R(1)$ and $R(2)$ of all the cells in the vicinity of the axis of symmetry are computed by assuming that these cells have rectangular cross-section:

$$\Delta Z(1,j) \;=\; V(1,j) \,/\, S(1,j) \;,\;\; 1 \leq j \leq J \;, \tag{29}$$

$$\Delta Z(2,j) \;=\; \Delta Z(1,j) \;,\;\; 1 \leq j \leq J \;. \tag{30}$$

(e) In the general case, the heights ΔZ at $R(i)$ and $R(i+1)$ for a given cell can depend on its distance from the axis of symmetry. The elementary volume of a trapezoidal ring can be expressed as:

$$V(i,j) \;=\; C_1 \; \Delta Z(i,j) \;+\; C_2 \; \Delta Z(i+1,j) \;,\;\; 1 \leq i \leq I \;,\;\; 1 \leq j \leq J \tag{31}$$

$$C_1 \;=\; \left(\frac{2\;\pi}{R(i+1) \;-\; R(i)} \right) \times \left(\frac{1}{6}\; R(i+1)^3 \;+\; \frac{1}{3}\; R(i)^3 \;-\; \frac{1}{2}\; R(i+1)\; R(i)^2 \right) \tag{32}$$

$$C_2 \;=\; \left(\frac{2\;\pi}{R(i+1) \;-\; R(i)} \right) \times \left(\frac{1}{3}\; R(i+1)^3 \;+\; \frac{1}{6}\; R(i)^3 \;-\; \frac{1}{2}\; R(i)\; R(i+1)^2 \right) \;; \tag{33}$$

hence, the height at $R(i+1)$ is obtained from that at $R(i)$:

$$\Delta Z(i+1,j) \;=\; \left(V(i,j) \;-\; C_1\; \Delta Z(i,j) \right) / \, C_2 \;\;,\;\; 1 \leq i \leq I \;,\;\; 1 \leq j \leq J \;. \tag{34}$$

(f) Axial coordinates of the cell vertices can be computed straightforwardly:

$$Z(i,j+1) \;=\; Z(i,j) \;+\; \Delta Z(i,j)\;, \quad 1 \le i \le I\;, \quad 1 \le j < J\;, \tag{35}$$

wherein $Z(i,1) = 0$ (plane of symmetry).
(g) Finally, the cell's position $[r(i),\; z(i,j)]$ is updated from the vertices coordinates:

$$r(i) \;=\; (\,R(i) \;+\; R(i+1)\,)\,/\,2 \quad , \quad 1 \le i \le I\;, \tag{36}$$

$$\begin{aligned} z(i,j) \;=\; (\,Z(i,j) \;+\; Z(i+1,j) \\ \;+\; Z(i,j+1) \;+\; Z(i+1,j+1)\,)\,/\,4 \quad , \quad 1 \le i \le I\;, \quad 1 \le j \le J\;. \end{aligned} \tag{37}$$

The algorithm was written in Python language, and no attempts were conducted in optimizing it.

NOMENCLATURE	
a_w	water activity in the product
C	Guggenheim constant (GAB model)
$C_{P,\,air}$	air heat capacity [J/kg/K]
$C^{\#}_{P,\,dm}$	intrinsic heat capacity of dry matter [J/kg-dm/K]
$C^{\#}_{P,\,w}$	intrinsic heat capacity of water [J/kg-w/K]
D	diameter of the product slice [m]
$D^\star = D/D_0$	dimensionless diameter
D_0	initial diameter of the product slice [m]
D_w	water diffusivity in the product [m^2/s]
$D_{w,dry,ref}$	water diffusivity in very dry material at temperature T_{ref} [m^2/s]
$D_{w,wet,ref}$	water diffusivity in very wet material at temperature T_{ref} [m^2/s]
E_{dry}	activation energy value for diffusion in very dry material [J/mol]
E_{wet}	activation energy value for diffusion in very wet material [J/mol]
h	heat transfer coefficient at air-product interfaces [W/m^2/K]
H	height of the product slice [m]
H_0	initial height of the product slice [m]
i	column index of cell position
I	number of columns assumed in meshing the domain
j	line index of cell position
J	number of lines assumed in meshing the domain
$\vec{j}_q$	energy flux relative to the dry matter [W/m^2]
$\vec{j}_{w/dm}$	water flux relative to the dry matter [kg-w/m^2/s]
k	mass transfer coefficient at the air-product interfaces [m/s]
K	correction factor (GAB model)
Le	Lewis number
L_v	latent heat of water vaporization [J/kg]
$\vec{n}$	surface normal unit vector
$r(i)$	bulk position of the cell along the radial direction [m]
$R(i)$	(i)-th position of the cell along the radial direction [m]
$R_0 = D_0/2$	initial width ("radius") of the computational domain [m]
RH_{air}	air relative humidity [%]
S	surface of the product slice [m^2]
$S^\star = S/S_0$	dimensionless surface of the product slice
S_0	initial surface of the product slice [m^2]
t	time [s]
T	temperature [K]
T_0	initial temperature [K]
T_{air}	air temperature [K]
T_{ref}	reference temperature [K]
T_{wb}	wet-bulb temperature [K]
u	internal energy of the product per kg of dry matter (J/kg-dm)
u_{dm}	internal energy of dry matter in the product (J/kg-dm)
u_w	internal energy of water in the product (J/kg-w)
$\vec{v}_{dm}$	dry matter velocity in the product [m/s]

Continuation of NOMENCLATURE	
V	volume of the product slice [m^3]
$V^\star = V/V_0$	dimensionless volume of the product
V_0	initial volume of the product slice [m^3]
X_w	local water content [kg-w/kg-dm]
$\overline{X}_w$	average water content in the food matrix [kg-w/kg-dm]
$\overline{X}_w^\star = \overline{X}_w/X_{w,0}$	dimensionless water content
$X_{w,0}$	initial water content in the product [kg-w/kg-dm]
$X_{w,mono}$	mono-layer water content [kg-w/kg-dm] (GAB model)
$z(i,j)$	bulk position of the cell along the axial direction [m]
$Z(i,j)$	(i,j)-th position of the cell along the axial direction [m]
$Z_0 = H_0/2$	initial height of the computational domain [m]
α	volume fraction occupied by dry matter in the product
β	exponent, power-law relying dimensionless diameter and volume
$\Delta R(i)$	distance between the radial ordinates of two corners of a cell [m]
$\Delta S(i)$	surface between two successive radial ordinates of a cell [m^2]
Δt	time step [s]
$\Delta T(i,j)$	variation in the temperature in a given cell [K]
$\Delta X_w(i,j)$	variation in the water content in a given cell [kg-w/kg-dm]
$\Delta Z(i,j)$	distance between the axial ordinates of two corners of a cell [m]
λ	product thermal conductivity [W/m/K]
λ_{dm}	dry matter thermal conductivity [W/m/K]
λ_w	liquid water thermal conductivity [W/m/K]
ρ_{air}	air mass density [kg/m^3]
ρ_{dm}	mass density of dry matter (mass of dry matter per total volume) [kg-dm/m^3]
$\rho_{dm,0}$	initial mass density of dry matter [kg-dm/m^3]
$\rho_{dm}^{\#}$	intrinsic mass density of dry matter (mass of dry matter per volume of dry matter) [kg-dm/m^3-dm]
$\rho_{v,sat}$	mass density of saturated water vapor [kg-w/m^3]
$\rho_w^{\#}$	intrinsic mass density of liquid water (mass of water per volume of water) [kg-w/m^3-w]
ϕ_R	water mass flow along the radial direction [kg-w/s]
ϕ_Z	water mass flow along the axial direction [kg-w/s]
Φ_R	heat flow along the radial direction [J/s]
Φ_Z	heat flow along the axial direction [J/s]

Table 1 Experimental drying operating conditions and key model parameters considered in numerical simulations (I).

	case A	case B	case C	case D	
• pilot unit operating conditions:					
air temperature T_{air} [°C]	60	60	50	50	([1])
air relative humidity RH_{air} [%]	20	30	20	30	([1])
wet-bulb temperature T_{wb} [°C]	35.3	40.0	28.7	32.6	
dew-point temperature T_d [°C]	28.9	36.1	20.9	27.7	
• typical values before experiments:					
slice temperature T_0 [°C]	20				([1])
slice water content $X_{w,0}$ [kg-w/kg-dm]	11				([1])
slice height H_0 [m]	0.007				([1])
slice radius R_0 [m]	0.02				([1])
• typical values after experiments:					
characteristic drying time $1/\left(d\overline{X}_w/dt\right)_{t=0}$ [s]	1.42 10^{-4}	1.30 10^{-4}	1.15 10^{-4}	1.05 10^{-4}	([1])
drying time $t_{1/2}$ (when $\overline{X}_w^\star = 1/2$) [min]	76	80	88	94	
drying time $t_{1/8}$ (when $\overline{X}_w^\star = 1/8$) [min]	190	183	227	231	
• estimates from laboratory experiments:					
GAB parameter C	1.45		1.17		([1])
GAB parameter K	0.984		0.970		([1])
GAB parameter $X_{w,mono}$ [kg-w/kg-dm]	0.116		0.137		([1])

[1] As reported by Marques *et al.* (2022).

Table 2 Experimental drying operating conditions and key model parameters considered in numerical simulations (II).

	case A	case B	case C	case D	
• heat and mass transfer parameters:					
heat transfer coefficient h [W/m^2/K]	33	37	31	35	([2])
ratio of transfer coefficients k/h for mass and heat		$1.02\ 10^{-3}$			([2])
latent heat of vaporization L_v [J/kg] at 60 °C		$2.36\ 10^{6}$			
• pure water properties:					
density $\rho_w^\#$ [kg/m^3]		991			
heat capacity $C_{P,\,w}^\#$ [J/kg/K]		4180			
thermal conductivity $\lambda_w^\#$ [W/m/K]		0.631			
• dry matter properties:					
density $\rho_{dm}^\#$ [kg/m^3]		1590			([3])
heat capacity $C_{P,\,dm}^\#$ [J/kg/K]		1620			([3])
thermal conductivity $\lambda_{dm}^\#$ [W/m/K]		0.250			([3])
• mesh and time step:					
mesh (number of lines, number of columns)		$J = 5, \quad I = 6 \times J = 30$			([4])
time step		$\Delta\, t = 0.01$ s			([4])

[2] See Section 2.

[3] Data provided by Hermann *et al.* (1999) about nine accessions of fresh yacón allowed us to estimate the averaged composition: 0.37g/100g for proteins, 0.024g/100g for fat, 11g/100g for carbohydrates, 0.36g/100g for fibers, and 0.51g/100g for ash. These values were considered in applying Choi and Oikos' (1986) approach for estimating yacón thermal properties at the temperature of 40 °C. The latter represents the average between the slice initial temperature 20 °C and the reference temperature 60 °C.

[4] 'Ad hoc' compromise between reliability of model predictions and computational cost (typically, 4 hours on a 11 Gen Intel Core i7-1165G7 at 2.8 GHz, 16 Gb-RAM laptop).

Table 3 Influence of key physical parameters. Percentage changes refer to the values assumed in case A. Last columns indicate departures Δt_f between drying times t_f identified in model predictions and in observations (see Table 1).

case	T_{air} [°C]	RH_{air} [%]	$D_{w,dry,ref}$ [m^2/s]	$D_{w,wet,ref}$ [m^2/s]	$E_{dry} = E_{wet}$ [kJ/mol]	h [W/m^2/K]	$\Delta t_{1/2}$ [min]	$\Delta t_{1/8}$ [min]
A	60	20	$1\ 10^{-12}$	$1.6\ 10^{-10}$	30	33	+4	−3
A1	60	20	**−50%**	$1.6\ 10^{-10}$	30	33	+4	−3
A2	60	20	**−10%**	$1.6\ 10^{-10}$	30	33	+4	−3
A3	60	20	**+10%**	$1.6\ 10^{-10}$	30	33	+4	−3
A4	60	20	**+50%**	$1.6\ 10^{-10}$	30	33	+4	−3
A5	60	20	$1\ 10^{-12}$	**−50%**	30	33	+25	+96
A6	60	20	$1\ 10^{-12}$	**−10%**	30	33	+4	+6
A7	60	20	$1\ 10^{-12}$	**+10%**	30	33	+3	−10
A8	60	20	$1\ 10^{-12}$	**+50%**	30	33	−1	−28
A9	60	20	$1\ 10^{-12}$	$1.6\ 10^{-10}$	**−50%**	33	−1	−24
A10	60	20	$1\ 10^{-12}$	$1.6\ 10^{-10}$	**−10%**	33	+3	−7
A11	60	20	$1\ 10^{-12}$	$1.6\ 10^{-10}$	**+10%**	33	+6	+2
A12	60	20	$1\ 10^{-12}$	$1.6\ 10^{-10}$	**+50%**	33	+12	+21
A13	60	20	$1\ 10^{-12}$	$1.6\ 10^{-10}$	30	**−50%**	+70	+111
A14	60	20	$1\ 10^{-12}$	$1.6\ 10^{-10}$	30	**−20%**	+20	+24
A15	60	20	$1\ 10^{-12}$	$1.6\ 10^{-10}$	30	**−10%**	+11	+9
A16	60	20	$1\ 10^{-12}$	$1.6\ 10^{-10}$	30	**+10%**	−2	−13
A17	60	20	$1\ 10^{-12}$	$1.6\ 10^{-10}$	30	**+20%**	−6	−20
A18	60	20	$1\ 10^{-12}$	$1.6\ 10^{-10}$	30	**+50%**	−16	−35
B	**60**	**30**	$1\ 10^{-12}$	$1.6\ 10^{-10}$	30	**37**	+6	+10
C	**50**	**20**	$1\ 10^{-12}$	$1.6\ 10^{-10}$	30	**31**	+11	+10
D	**50**	**30**	$1\ 10^{-12}$	$1.6\ 10^{-10}$	30	**35**	+10	+12

Figure Captions

Figure 1. Schematic view of a cylindrical food slice, before any drying (left) and later on (right), according to a 2D axis-symmetrical representation. Axial distances (z) are measured from the plane of symmetry that subdivides the cylinder into two identical halves; radial distances (r) are measured from the the cylinder axis. A elementary volume of this cylinder is put in evidence, characterized by its height δz and width δr; its horizontal surface δS equals $2\,\pi\, r\,\delta r$.

Figure 2. **(a)** Dimensionless water content evolution under the reference drying operating condition [air flow 4 m/s, T_{air} = 60 °C, RH_{air} = 20 %], as provided by observations (Marques *et al.*, 2022) and model predictions. Two selected drying times are identified, corresponding respectively to 1/2 and 1/8 of the initial water content as resulting from observations. **(b)** Influence

of the time step Δt assumed in model simulations on selected drying times; the grey line indicate values from observations. **(c)** Influence of the number of mesh elements $I \times J$ assumed in model simulations on selected drying times. Stars indicate results corresponding to case A simulations (time step = 0.01 s, number of mesh elements = 150).

Figure 3. Influence of selected model parameters on predictions of drying times $t_{1/2}$ and $t_{1/8}$: **(a)** water diffusivity in very dry material, **(b)** water diffusivity in very wet material, **(c)** energy of activation, and **(d)** heat transfer coefficient. Values of $t_{1/2}$ and $t_{1/8}$ from observations are indicated. Stars indicate results corresponding to case A simulations ($D_{w,dry,ref} = 10^{-12}$ m^2/s, $D_{w,wet,ref} = 1.6\ 10^{-10}$ m^2/s, $E_{dry} = E_{wet} = 30$ kJ/mol, $h = 33$ W/m^2/K).

Figure 4. Temperature, water content, water diffusivity and water activity fields in the food slice at selected times. Dimensions of the food slice are expressed in meters. Positions 1 and 2 considered in Figure 5 are also displayed.

Figure 5. Evolution of selected variables according to model predictions under the reference drying operating conditions (air flow 4 m/s, $T_{air} = 60$ °C, RH_{air} = 20 %): at the surface (1) and at the core (2).

Figure 6. Evolution of selected variables according to model predictions (black lines) and to observations of mass loss (colored lines and black symbols), under the reference drying operating conditions (air flow 4 m/s, $T_{air} = 60$ °C, $RH_{air} = 20$ %). Arrows recall the decrease of selected variables as the drying progresses.

Figure 7. Dimensionless water content evolution under the four drying conditions studied by Marques *et al.* (2022), as provided by observations and model predictions.

Figure 8. Schematic view of a elementary volume of the food matrix, in its 2D axi-symmetric representation.

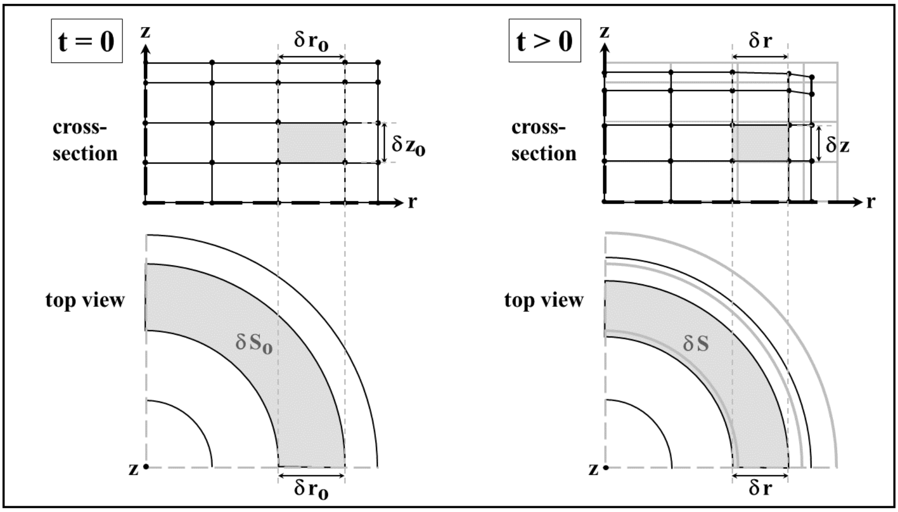

Fig. 1 Schematic view of a cylindrical food slice, before any drying (left) and later on (right), according to a 2D axi-symmetrical representation. Axial distances (z) are measured from the plane of symmetry that subdivides the cylinder into two identical halves; radial distances (r) are measured from the the cylinder axis. An elementary volume of this cylinder is put in evidence, characterized by its height δz and width δr; its horizontal surface δS equals $2\,\pi\,r\,\delta r$.

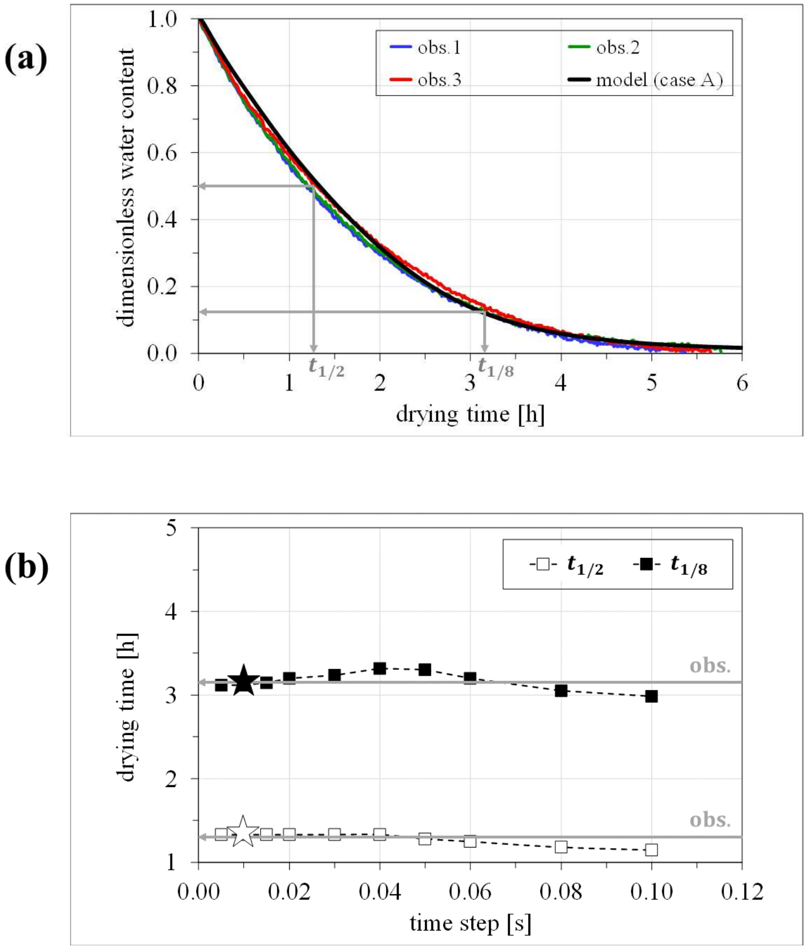
(a)
1.0
0.8
0.6
0.4
0.2
0.0
dimensionless water content
obs.1
obs.2
obs.3
model (case A)
$t_{1/2}$
$t_{1/8}$
0
1
2
3
4
5
6
drying time [h]
(b)
5
4
3
2
1
drying time [h]
$t_{1/2}$
$t_{1/8}$
obs.
obs.
0.00
0.02
0.04
0.06
0.08
0.10
0.12
time step [s]

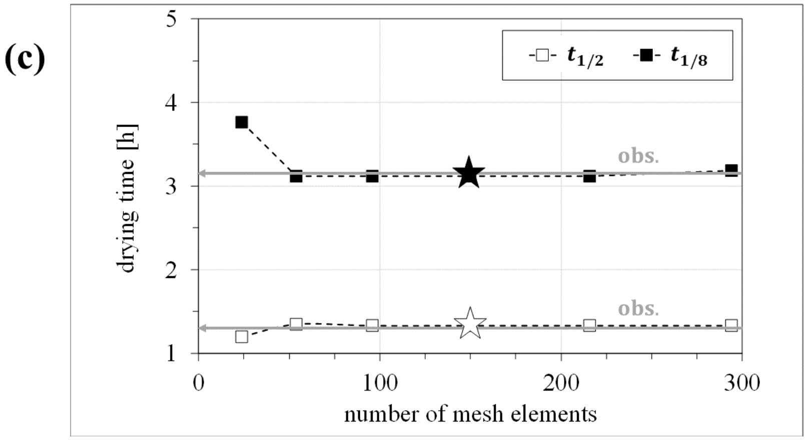

Fig. 2 **(a)** Dimensionless water content evolution under the reference drying operating condition [air flow 4 m/s, T_{air} = 60 °C, RH_{air} = 20 %], as provided by observations (Marques *et al.*, 2022) and model predictions. Two selected drying times are identified, corresponding respectively to 1/2 and 1/8 of the initial water content as resulting from observations. **(b)** Influence of the time step Δt assumed in model simulations on selected drying times; the grey line indicate values from observations. **(c)** Influence of the number of mesh elements $I \times J$ assumed in model simulations on selected drying times. Stars indicate results corresponding to case A simulations (time step = 0.01 s, number of mesh elements = 150).

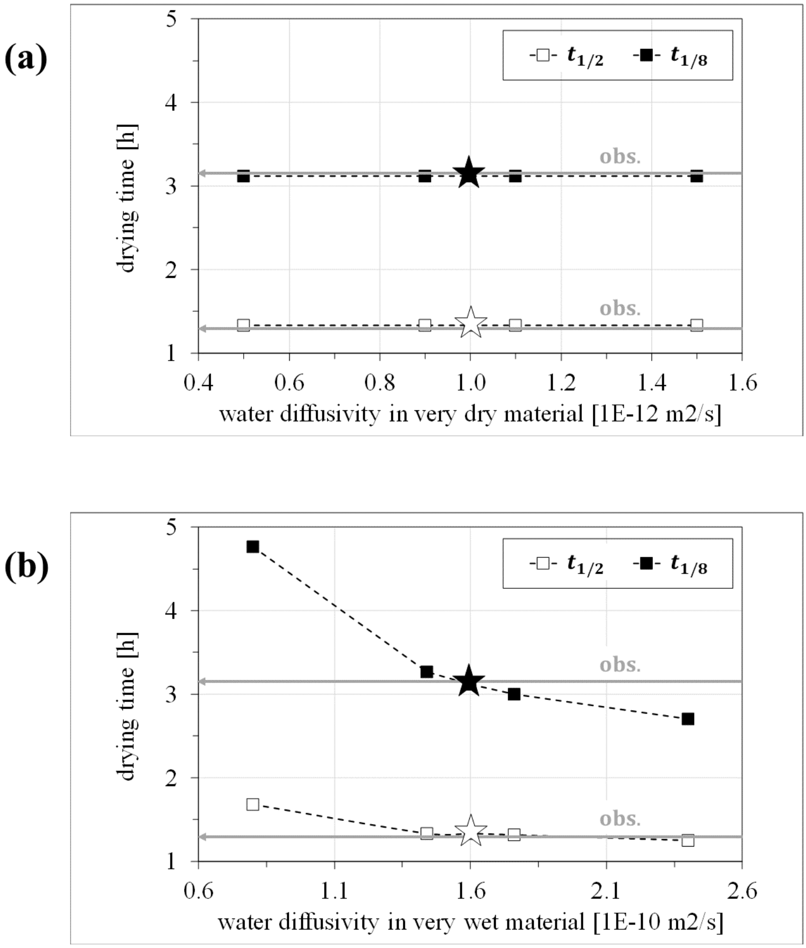
(a)
5
4
3
2
1
drying time [h]
-□- $t_{1/2}$ -■- $t_{1/8}$
obs.
obs.
0.4 0.6 0.8 1.0 1.2 1.4 1.6
water diffusivity in very dry material [1E-12 m2/s]
(b)
5
4
3
2
1
drying time [h]
-□- $t_{1/2}$ -■- $t_{1/8}$
obs.
obs.
0.6 1.1 1.6 2.1 2.6
water diffusivity in very wet material [1E-10 m2/s]

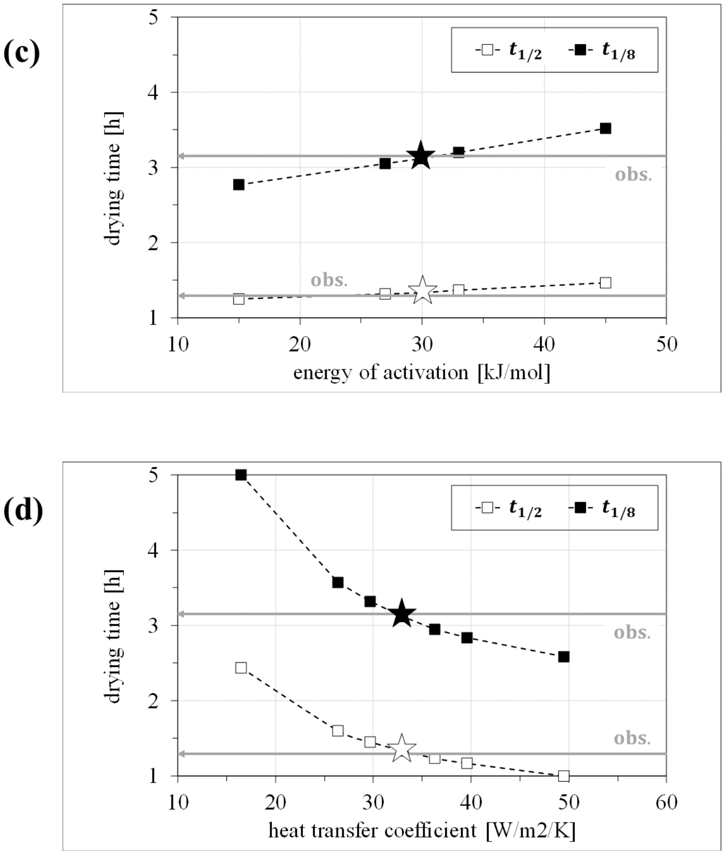

Fig. 3 Influence of selected model parameters on predictions of drying times $t_{1/2}$ and $t_{1/8}$: **(a)** water diffusivity in very dry material, **(b)** water diffusivity in very wet material, **(c)** energy of activation, and **(d)** heat transfer coefficient. Values of $t_{1/2}$ and $t_{1/8}$ from observations are indicated. Stars indicate results corresponding to case A simulations ($D_{w,dry,ref} = 10^{-12}$ m^2/s, $D_{w,wet,ref} = 1.6\ 10^{-10}$ m^2/s, $E_{dry} = E_{wet} = 30$ kJ/mol, $h = 33$ W/m^2/K).

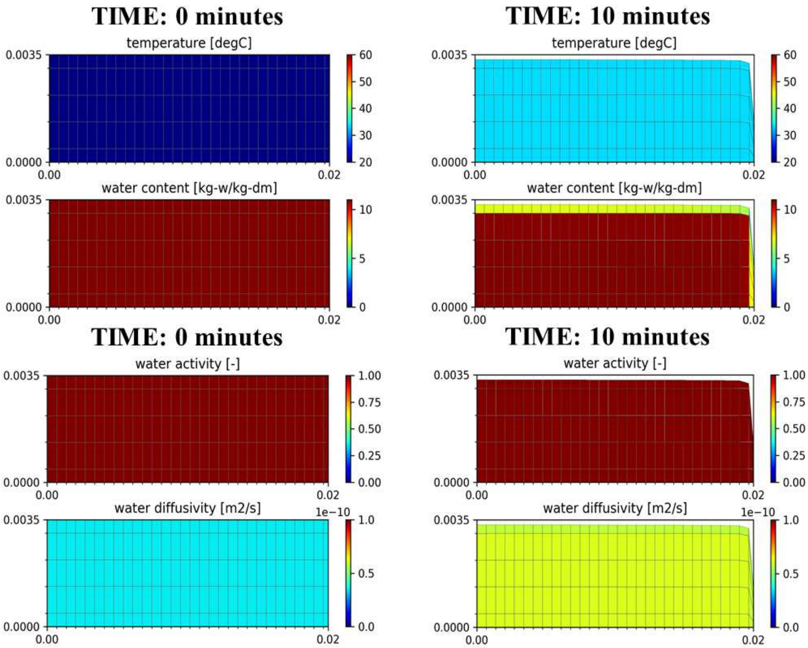
TIME: 0 minutes
temperature [degC]
water content [kg-w/kg-dm]
TIME: 0 minutes
water activity [-]
water diffusivity [m2/s]
TIME: 10 minutes
temperature [degC]
water content [kg-w/kg-dm]
TIME: 10 minutes
water activity [-]
water diffusivity [m2/s]
0.0035
0.0000
0.00
0.02
1e−10

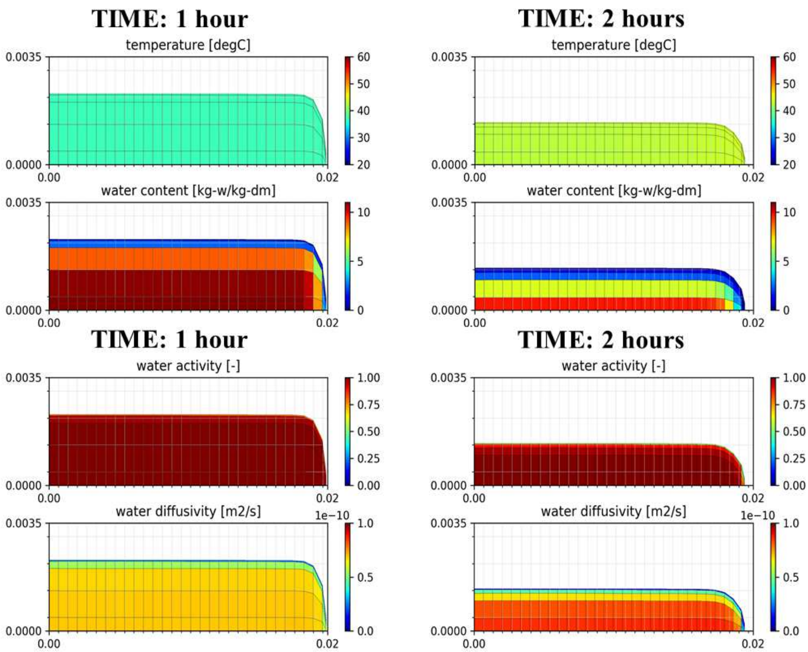
TIME: 1 hour
temperature [degC]
water content [kg-w/kg-dm]
TIME: 1 hour
water activity [-]
water diffusivity [m2/s]
TIME: 2 hours
temperature [degC]
water content [kg-w/kg-dm]
TIME: 2 hours
water activity [-]
water diffusivity [m2/s]
0.0035
0.0000
0.00
0.02
1e−10

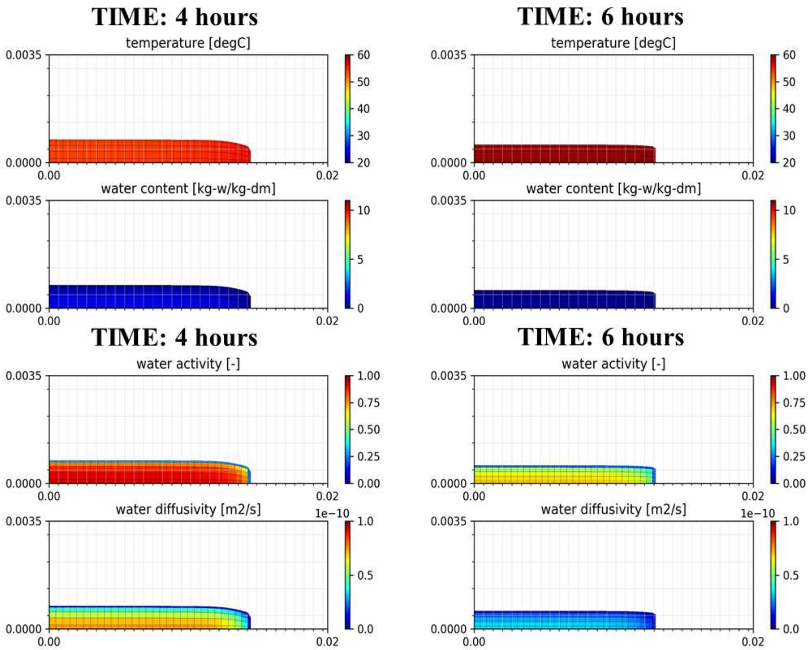

Fig. 4 Temperature, water content, water diffusivity and water activity fields in the food slice at selected times. Dimensions of the food slice are expressed in meters. Positions 1 and 2 considered in Figure 5 are also displayed.

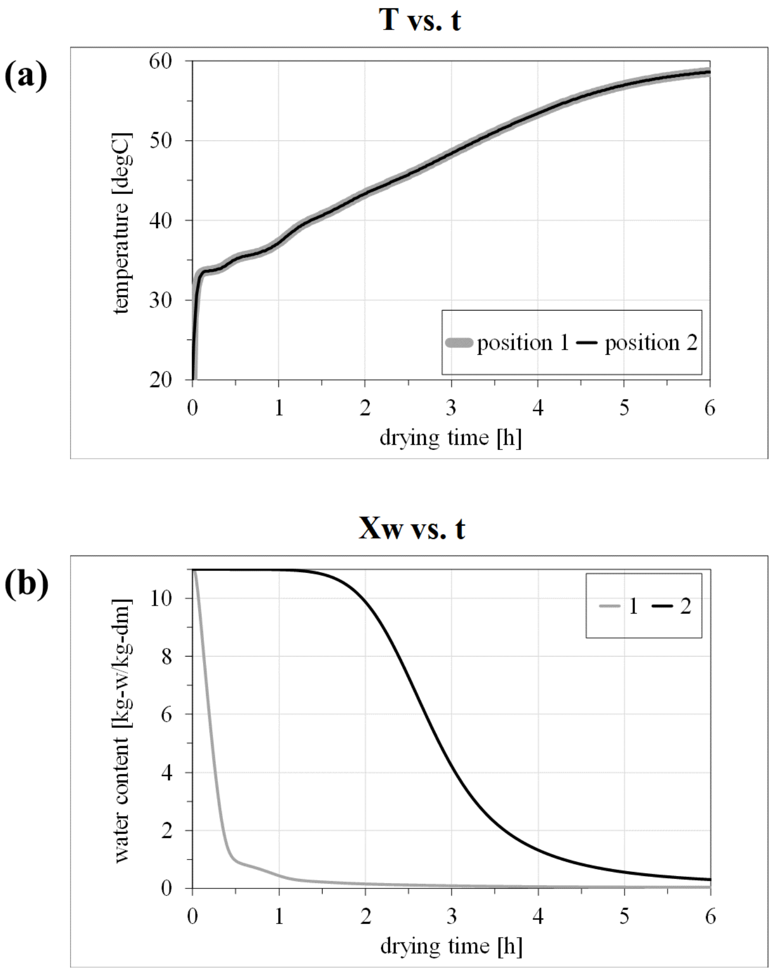
T vs. t
(a)
temperature [degC]
60
50
40
30
20
position 1
position 2
0
1
2
3
4
5
6
drying time [h]
Xw vs. t
(b)
water content [kg-w/kg-dm]
10
8
6
4
2
0
1
2
0
1
2
3
4
5
6
drying time [h]

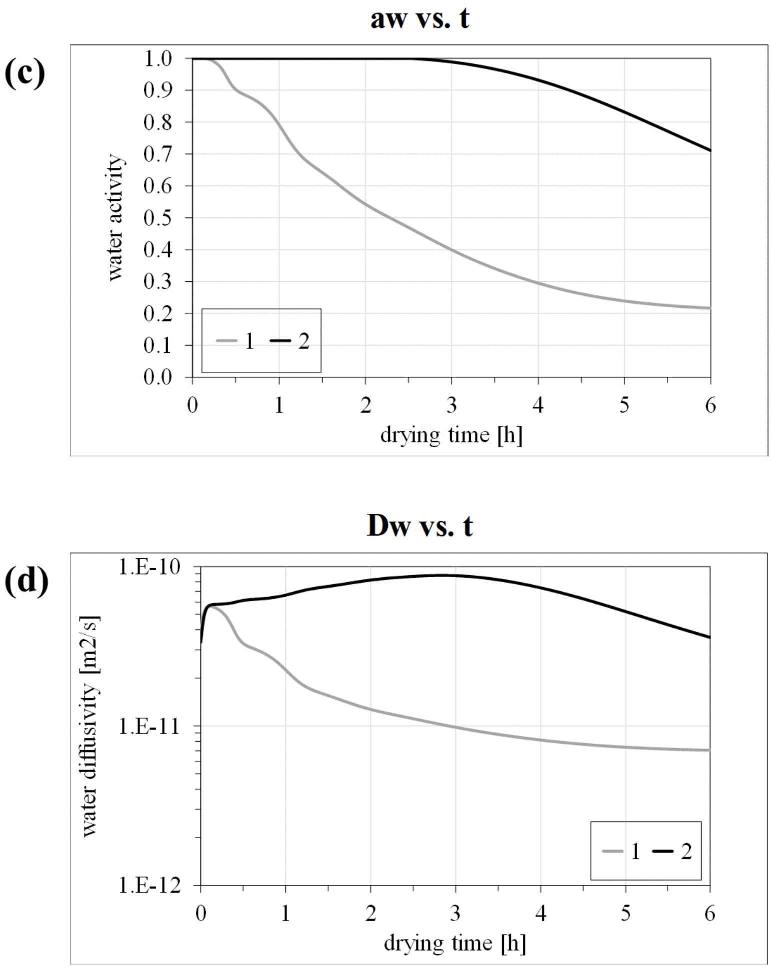

Fig. 5 Evolution of selected variables according to model predictions under the reference drying operating conditions (air flow 4 m/s, T_{air} = 60 °C, RH_{air} = 20 %): at the surface (1) and at the core (2).

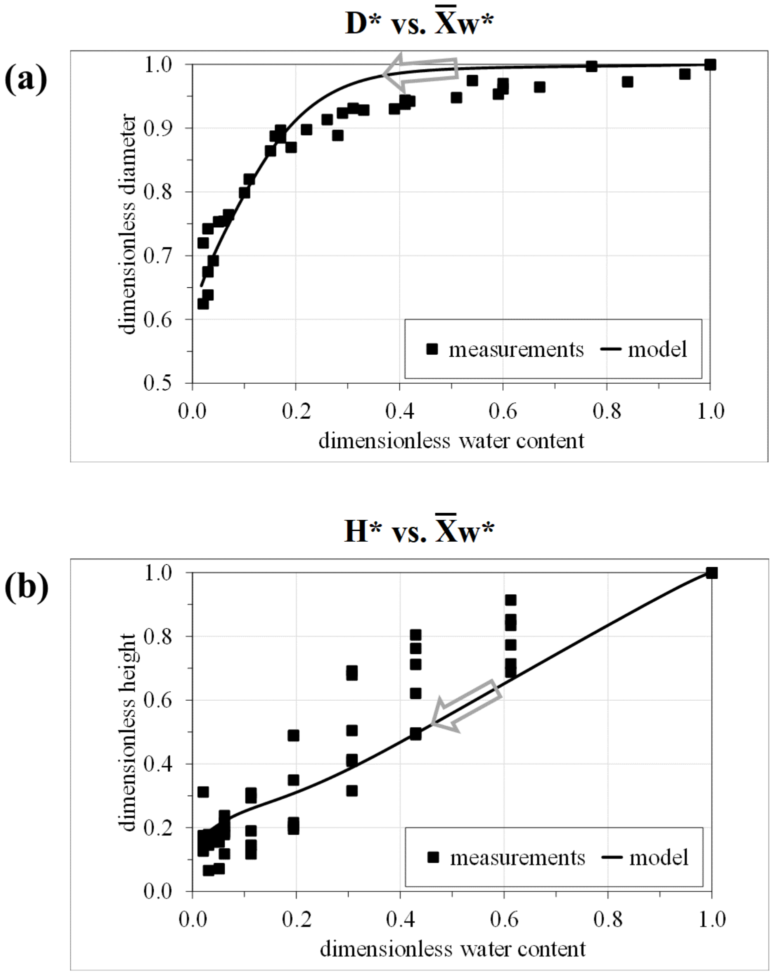
D* vs. $\overline{X}$w*
(a)
1.0
0.9
0.8
0.7
0.6
0.5
dimensionless diameter
0.0
0.2
0.4
0.6
0.8
1.0
dimensionless water content
measurements
model
H* vs. $\overline{X}$w*
(b)
1.0
0.8
0.6
0.4
0.2
0.0
dimensionless height
0.0
0.2
0.4
0.6
0.8
1.0
dimensionless water content
measurements
model

(c)

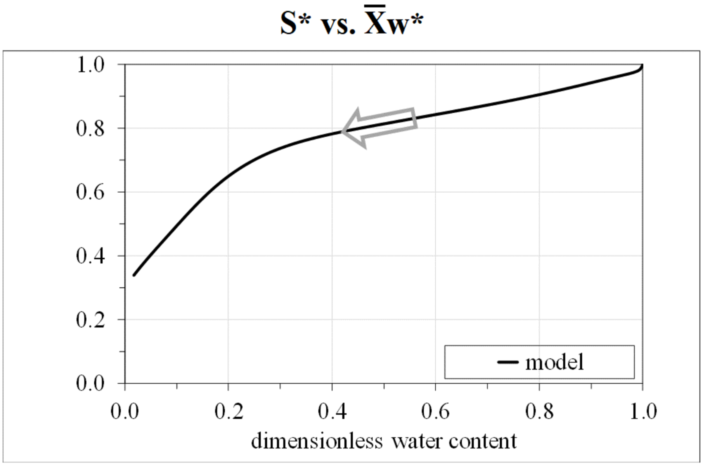
S* vs. $\overline{X}$w*
1.0
0.8
0.6
0.4
0.2
0.0
0.0
0.2
0.4
0.6
0.8
1.0
dimensionless water content
model

(d)

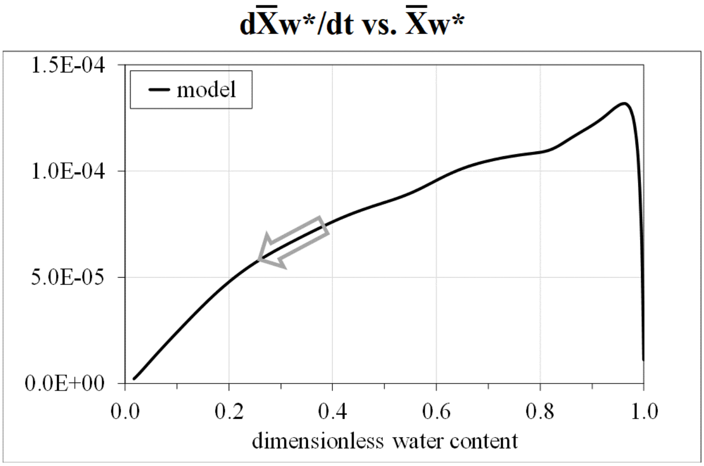
d$\overline{X}$w*/dt vs. $\overline{X}$w*
1.5E-04
1.0E-04
5.0E-05
0.0E+00
0.0
0.2
0.4
0.6
0.8
1.0
dimensionless water content
model

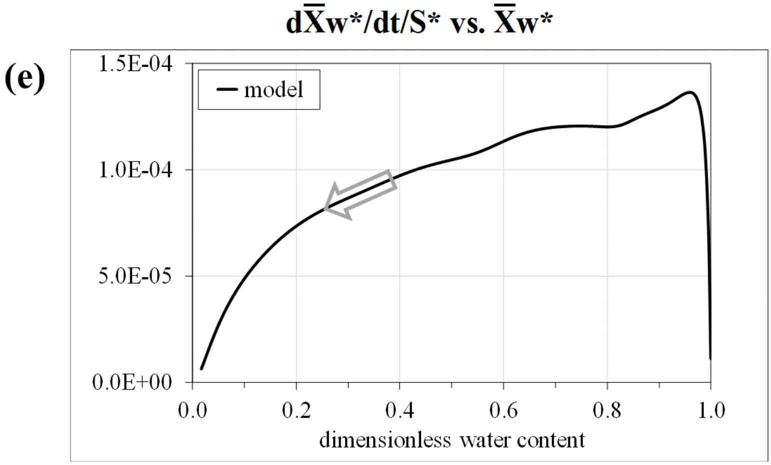

Fig. 6 Evolution of selected variables according to model predictions (black lines) and to observations of mass loss (colored lines and black symbols), under the reference drying operating conditions (air flow 4 m/s, T_{air} = 60 °C, RH_{air} = 20 %). Arrows recall the decrease of selected variables as the drying progresses.

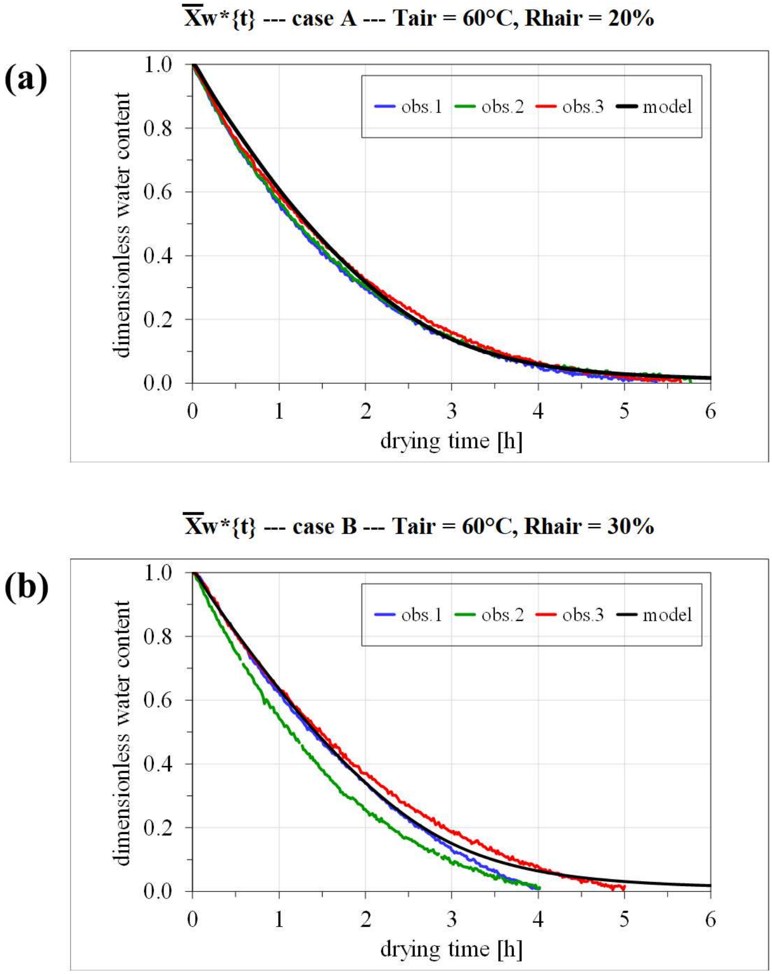
Xw*{t} --- case A --- Tair = 60°C, Rhair = 20%
(a)
obs.1
obs.2
obs.3
model
dimensionless water content
drying time [h]
Xw*{t} --- case B --- Tair = 60°C, Rhair = 30%
(b)
obs.1
obs.2
obs.3
model
dimensionless water content
drying time [h]

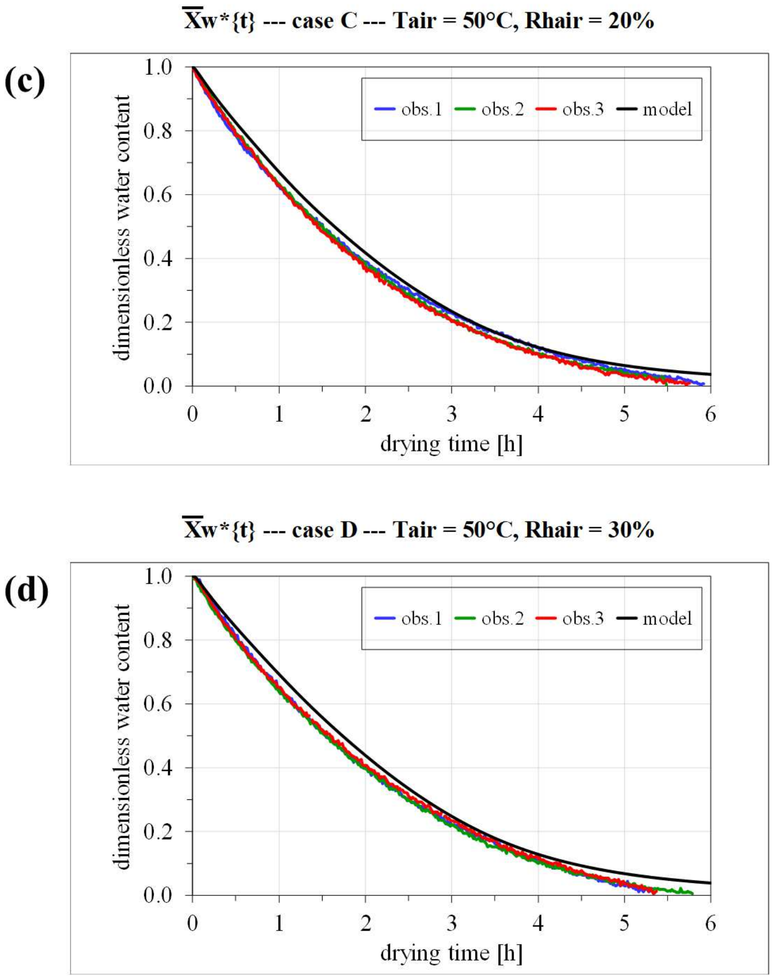

Fig. 7 Dimensionless water content evolution under the four drying conditions studied by Marques *et al.* (2022), as provided by observations and model predictions.

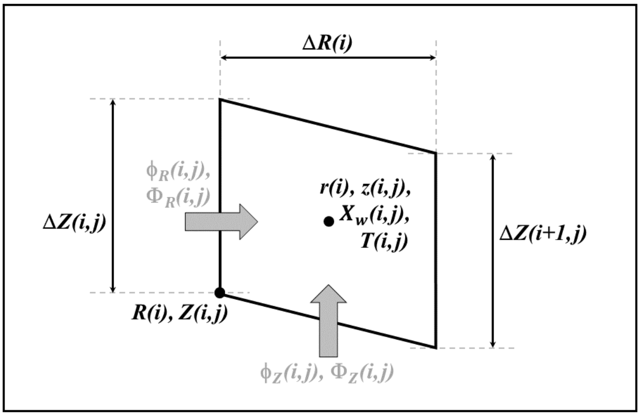

Fig. 8 Schematic view of an elementary volume of the food matrix, in its 2D axi-symmetric representation.